https://doi.org/10.5194/egusphere-2026-953
Preprint. Discussion started: 26 March 2026

[heloise.guilluy@univ-grenoble-alpes.fr]

Investigating the relationship between Total Air Content (TAC) variations in polar ice cores and local surface climate conditions

Héloïse Guilluy[1], Émilie Capron[1], Frédéric Parrenin[1], Vladimir Lipenkov[2], Jochen Schmitt[3], Patricia Martinerie[1], Zhipeng Wu[4], Qiuzhen Yin[4], Anna Klüssendorf[5], Amaëlle Landais[5], Barbara Seth[3], Hubertus Fischer[3], and Dominique Raynaud[1]

[1]Institute of Environmental Geoscience (IGE), Univ. Grenoble Alpes, CNRS, IRD, INRAE, Grenoble-INP, 38000 Grenoble, France
[2]Climate and Environmental Research Laboratory, Arctic and Antarctic Research Institute, Saint Petersburg, 199397, Russia
[3]Climate and Environmental Physics, Physics Institute, and Oeschger Centre for Climate Change Research, University of Bern, Bern, Switzerland
[4]Earth and Life Institute, Earth and Climate Research Center, Université catholique de Louvain, 1348 Louvain-la-Neuve, Belgium
[5]Laboratoire des Sciences du Climat et de l'Environnement, UMR8212, CNRS – Gif sur Yvette, France

Abstract. While air bubbles in polar ice cores are well known for archiving past atmospheric composition, the quantity of air trapped in these bubbles also carries significant paleoclimatic information. This parameter, known as Total Air Content (TAC), was first used to reconstruct past ice sheet elevation and later became an orbital dating tool after its temporal variations revealed a strong correlation with local summer insolation. However, limited understanding of relationships between TAC, pore volume at close-off depth, and surface parameters has restricted its widespread use. In this study, we investigate the link between surface parameters (e.g. temperature and accumulation) and changes in TAC at both spatial and temporal scales in order to better understand TAC as an environmental proxy and as an orbital dating tool. To do so, we first present a new dataset extending the TAC record from the EPICA Dome C (EDC) ice core back to 800 ka, as well as new TAC records from the TALDICE and EDML ice cores covering the last glacial-interglacial cycle. Second, we combine these new datasets with a compilation of published TAC data from ice cores across Antarctica and Greenland to explore the influence of surface climate parameters controlling the changes in TAC both at spatial and temporal scales. Our spatial-scale analysis first examines how recent TAC values relate to atmospheric pressure and elevation. We then investigate pore volume at close-off (i.e. TAC values corrected for ideal gas law effects) to assess the influence of mean annual temperature, accumulation rate, and local summer insolation. We evidence a strong correlation between the pore volume at close-off and local half year summer insolation for East Antarctic sites, suggesting a direct control of local insolation on firn densification in this region. Temporal-scale analyses on TAC records covering at least 40 ka confirm that TAC records contain an orbital-scale signature of local insolation but also show that local summer insolation alone cannot capture the full TAC variability. Multiple regression analysis incorporating local insolation and reconstructed surface temperatures or accumulation better predicts TAC temporal changes, particularly during glacial terminations. Our new EDC high-resolution record also revealed significant millennial-scale TAC changes during these glacial terminations. Hence, our results highlight that in addition to the orbital-scale impact of local summer insolation,

https://doi.org/10.5194/egusphere-2026-953
Preprint. Discussion started: 26 March 2026

millennial-to-multi-millennial-scale changes in surface climate parameters also influence the temporal-scale TAC changes. Our findings suggest that orbital tuning between TAC and local insolation that neglects surface climate controls could introduce age uncertainties of 1–5 ka, calling for surface climate-related corrections prior to TAC-based orbital dating.

1 Introduction

Polar ice cores constitute an invaluable natural archive for reconstructing past climate changes over glacial-interglacial timescales and preserve past climates information in different forms. The ice matrix records climate proxies such as water isotopes reflecting local surface temperature changes (Jouzel et al., 2007) or aerosol impurities informing on atmospheric circulation(Wolff et al., 2006) and firn densification (Hörhold et al., 2012), while air bubbles trapped within the ice provide direct information on past atmospheric composition, such as greenhouse gas concentrations (Loulergue et al., 2008; Bereiter et al., 2015).

Among these proxies, the Total Air Content (TAC), is the amount of air trapped in polar ice expressed as a volume at standard temperature and pressure (STP) of air serves as a unique proxy. Following the ideal gas law, TAC is directly controlled by three physical parameters: air pressure, temperature, and pore volume at bubble close-off depth (Raynaud and Lebel, 1979; Martinerie et al., 1992). This relationship is mathematically expressed as:

$$TAC = V_c \cdot \frac{P_c}{T_c} \cdot \frac{T_0}{P_0} \tag{1}$$

where TAC is the TAC volume per unit mass of ice, at reference temperature (T_0) and pressure (P_0). V_c, P_c and T_c correspond to the pore volume, air pressure, and temperature at close-off depth.

While temperature can be estimated using the water isotopic ratios (e.g. δ^{18}O of the ice) (Jouzel et al., 2007), TAC is linked to changes in V_c and P_c. Based on this theoretical dependency of TAC with P_c and the fact that atmospheric pressure decreases with altitude, TAC was used to reconstruct past ice sheet elevation (Raynaud and Lorius, 1973; Raynaud and Lebel, 1979). However, reliable TAC-based elevation reconstructions require an understanding of the control parameters on V_c. Observations of significant TAC drops during cold periods in the Camp Century ice core first suggested a potential temperature dependence of V_c (Raynaud and Lorius, 1973; Raynaud and Lebel, 1979). A major breakthrough came when Martinerie et al. (1992) compiled TAC measurements from different sites and highlighted that present-time V_c is partially controlled by firn temperature at close off T_c, with warmer conditions corresponding to higher porosity of the firn at close-off depth. Nevertheless, the uncertainty in the parametrisation of V_c, which depends on complex interactions with local climate parameters (e.g. temperature at close off, annual surface temperature, accumulation rates and local summer insolation) and firn densification processes, has remained a persistent limitation for using TAC as an elevation proxy (Martinerie et al., 1994; Raynaud et al., 1997, 2007; Delmotte et al., 1999; Eicher et al., 2016; NEEM community members, 2013; Vudayagiri et al., 2025).

These challenges limited the use of TAC until Raynaud et al. (2007) highlighted (i) similar spectral properties between the EDC TAC record (0-440 ka) and the integrated summer insolation (ISI) at 75°S and (ii) an anti-correlation between the

https://doi.org/10.5194/egusphere-2026-953
Preprint. Discussion started: 26 March 2026

two parameters at orbital timescales. Later work identified a dominant obliquity signal ($\sim$ 41 kyr) and a weaker precession signal ($\sim$ 23 kyr), consistent with an influence of insolation on snow metamorphism and firn densification processes at Vostok (Lipenkov et al., 2011). Recently, Raynaud et al. (2024) refined TAC's sensitivity to insolation at EDC by introducing the Half-Year Summer Insolation (HYSI) as the most appropriate insolation index.

Based on the relationship between TAC variations and local insolation changes, TAC-based orbital dating is particularly valuable to constrain the chronologies of the deep ice cores drilled at the low-accumulation sites from the East Antarctic plateau (Parrenin et al., 2007; Bouchet et al., 2023). The latest reference ice core chronology, AICC2023, incorporates 42 age markers based on the visual alignment between TAC and the local insolation time series over the last 800 ka.

However, interpreting TAC variations requires careful consideration of the relevant age scales for different controlling processes (Edwards and Epifanio, 2025). Local summer insolation influences surface snow metamorphism, imprinting its signal on the ice age scale, while the temperature control on V_c operates throughout the entire firn densification process. Since the firn column experiences progressive temperature changes as snow travels from the surface to close-off depth (typically over $\sim$ 2000 years at low-accumulation sites), the effective temperature controlling V_c corresponds approximately to an age between ice and gas age scales. This complexity contributes to the uncertainties (3–10 ka) attached to TAC-derived age markers in AICC2023 (Bouchet et al., 2023). A recent inter-comparison study using continuous wavelet transform analysis revealed that $\sim$ 74% of TAC variance relates to changes in close-off porosity (V_c) that are not linked to the mean annual surface temperature, of which only $\sim$ 44% (on average) attributable to insolation and $\sim$ 30% to non-orbital climate effects at Vostok and EDC (Khomyakova et al., 2025). Hence, these non-orbital-scale variations significantly impact dating accuracy during periods of weak orbital forcing, highlighting ongoing challenges in understanding all physical drivers of pore volume at close-off and the need to explore the relationship between TAC and present-day insolation patterns.

Local climate parameters are driving firn densification through compaction and snow grain metamorphism, controlling the timing and efficiency of air bubble closure and determining the TAC signal in ice cores (Raynaud and Lebel, 1979; Martinerie et al., 1988, 1992; Raynaud et al., 2007; Gregory et al., 2014; Eicher et al., 2016). Among the key climate drivers, surface temperature affects TAC through two opposing mechanisms. Higher temperatures directly reduce TAC via thermal gas expansion (ideal gas law), but indirectly increase TAC through pore volume at close-off (Martinerie et al., 1992; Raynaud et al., 2007). Summer insolation operates through seasonal solar heating of the upper meters from the surface distinct from mean annual temperature effects on the entire firn column. Higher insolation results in greater heating at the surface and creates strong temperature and vapour pressure gradients that enhance grain growth in the upper snow layers (Arnaud et al., 2000; Raynaud et al., 2007). Although the length of summer and accumulation rate (which determine the exposure time of surface snow) also play a role, it is mainly the intensity of solar radiation that controls the heating, the increase in snow temperature, and the water vapour concentration in snow pores necessary to support grain growth (Raynaud et al., 2007). These insolation-enhanced gradients are most pronounced in the surface layer (to $\sim$2 m depth), where the most rapid grain growth occurs (Gow, 1969). Deeper, the seasonal temperature variations attenuate and become negligible below $\sim$ 10 m depth. At cold sites like Vostok and EDC, snow temperatures below 2 m remain around -55$\pm$10°C year-round (Petit et al., 1999; Cuffey and Paterson, 2010), where vapour transport becomes ineffective for enhanced grain development, though normal crystal growth continues at a

https://doi.org/10.5194/egusphere-2026-953
Preprint. Discussion started: 26 March 2026

slower rate throughout the deeper firn column (Gow, 1969). While quantitative links between surface metamorphism and pore closure require further investigation (Freitag et al., 2004), studies suggested that these grain size changes are carried through the firn column such that higher summer insolation, through increased snow temperature and vapour pressure gradients, increases the size of snow grains in the first few meters of firn, which then decreases pore volume in these same layers as they reach bubble close-off, ultimately reducing TAC (Arnaud, 1997; Arnaud et al., 2000; Raynaud et al., 2007; Epifanio et al., 2023). This mechanism explains the inverse relationship between insolation and TAC at orbital scales observed in individual ice cores, although the spatial relationship between V_c and insolation across different sites in Antarctica and Greenland has not been explored yet.

Temperature affects atmospheric moisture capacity (Clausius-Clapeyron), contributing to temperature-accumulation correlations which complicate identifying how each parameter individually affects TAC. Accumulation rates fundamentally control the timeline of firn densification, with higher rates reducing the time duration until the close-off depth is reached and the age difference (Δ-age) between ice and trapped gas. Grain size in the upper firn, which influences pore closure, results from the interplay between temperature (affecting grain growth rate) and accumulation rate (affecting time available for growth) (Alley et al., 1982; Schwander and Stauffer, 1984; Edwards and Epifanio, 2025)). In the upper firn (first meters of the column), where seasonal temperature variations still penetrate, surface-driven metamorphism dominates grain evolution (Harris Stuart, 2024). In deeper firn, where seasonal temperature variations no longer extend, overburden pressure linked to accumulation rate variations, drives densification through recrystallization and sintering processes (Cuffey and Paterson, 2010). During this stage, coarse-grained layers densify more rapidly than fine-grained layers, explaining that initially denser fine-grained layers become less dense than coarser-grained layers (Hörhold et al., 2011). Finally, the densification process leads to air communication stopping at the lock-in depth (LID), although small pressure changes can still influence gas mixing until bubble close-off depth (Sowers et al., 1992; Buizert and Severinghaus, 2016). The timing and formation of V_c at the close-off depth can thus greatly vary depending on the site-specific firn densification. The mechanisms controlling V_c remain debated. Percolation theory predicts closure at a critical porosity (Stauffer et al., 1985), supported by X-ray tomography measurements (Schaller et al., 2017) for a limited number of sites, yet inter-site V_c-climate variations challenge this hypothesis (Martinerie et al., 1992). Firn densification processes vary with climate conditions, resulting in different pore volume signatures across sites and timescales. At the Greenlandic NGRIP site, despite warmer temperatures that should increase V_c (Martinerie et al., 1992), TAC decreases during Dansgaard-Oeschger warming events, suggesting that increased overburden pressure from higher accumulation compresses the firn and offsets the temperature effect (Eicher et al., 2016). Synchronous anti-correlation between TAC with methane and δ^{15}N indicates that surface climate signals transfer to close-off zones as fast as atmospheric composition changes (Eicher et al., 2016). At the low-accumulation Antarctic site South Pole (SP), Epifanio et al. (2023) found millennial-scale TAC variations positively correlated with reconstructed accumulation rates and firn thickness proxies (e.g. δ^{15}N), which could be explained by the fact that with increasing accumulation the duration of grain growth near the surface decreases, which leads to finer grains and, ultimately, to an increased pore volume at close-off (Courville et al., 2007; Gregory et al., 2014). Understanding how firn processes control pore volume at close-off (V_c) requires isolating the complex interactions among surface parameters such

https://doi.org/10.5194/egusphere-2026-953
Preprint. Discussion started: 26 March 2026

as local insolations, accumulation rates, annual mean temperatures, and seasonal temperature variations (Eicher et al., 2016; Epifanio et al., 2023; Raynaud et al., 2024).

Despite existing correlations with summer insolation and surface parameters (e.g., accumulation rates, temperatures), the mechanisms driving TAC remain poorly understood. In particular, the physical controls on pore volume changes requires further investigation. This study addresses these gaps by compiling published and unpublished TAC records from Antarctica and Greenland (Fig. 1.). Based on this new compilation, we examine TAC signals, and associated pore volume changes across spatial and temporal scales (from millennial to orbital) and investigate their relationship to local surface parameters, namely the local insolation, the surface temperature, and the accumulation rate.

2 Methodology

2.1 Ice core sites

This study presents a compilation of 38 published and unpublished TAC records from deep and shallow ice cores in Antarctica and Greenland (Fig. 1.; Table 1.).

Here we introduce unpublished data measured on deep ice cores at IGE (EDC: 440-800 ka) and at the University of Bern (EDC: 20-600 ka; EPICA Dronning Maud Land (EDML): 11-56 ka; Talos Dome (TALDICE): 0-151 ka). We also present new data from shallow ice cores measured at the University of Bern, they are encompassing B34, B37 and the Beyond EPICA Oldest Ice (BEOI) drilling sites. The unpublished datasets are presented in the result section (3.).

We analysed the published TAC data from the following deep ice core projects: the Greenland Ice core Project (GRIP), North Greenland Ice core Project (NGRIP) and REnland ice CAP project (RECAP) in Greenland and Dome Fuji (DF), EDC over the 0-440 ka time interval, South Pole (SP), Vostok and West Antarctic Ice Sheet Divide (WAIS) in Antarctica (Table 1.).

TAC data covering less than 40 ka (Table 1.) include Skytrain Ice Rise (SIR), Camp Century (CC), Mizuho, and unpublished data from shallow ice cores at Little Dome C, the Beyond EPICA Oldest Ice (BEOI) drilling site, B34 and B37. Greenland Ice Sheet Project 2 (GISP2) and North Greenland Eemian Ice Drilling (NEEM) datasets were compiled but not included in our spatial-scale study because they did not cover recent time intervals. Data compiled in Martinerie et al. (1992) are also incorporated for this compilation and include the following sites: BHJ, BHF, BHP, D-10, BHB, BHQ, DE08, BHD, Byrd, Camp Century (CC), Dome C, South Pole, Vostok. Data from Martinerie et al. (1994) include sites located along a traverse (Mirny-Vostok): KM-60, KM-73, KM-105, KM-140, KM-200, KM-260, KM-325, KM-369, KM-400 in addition to D-47 and EUROCORE sites.

https://doi.org/10.5194/egusphere-2026-953
Preprint. Discussion started: 26 March 2026

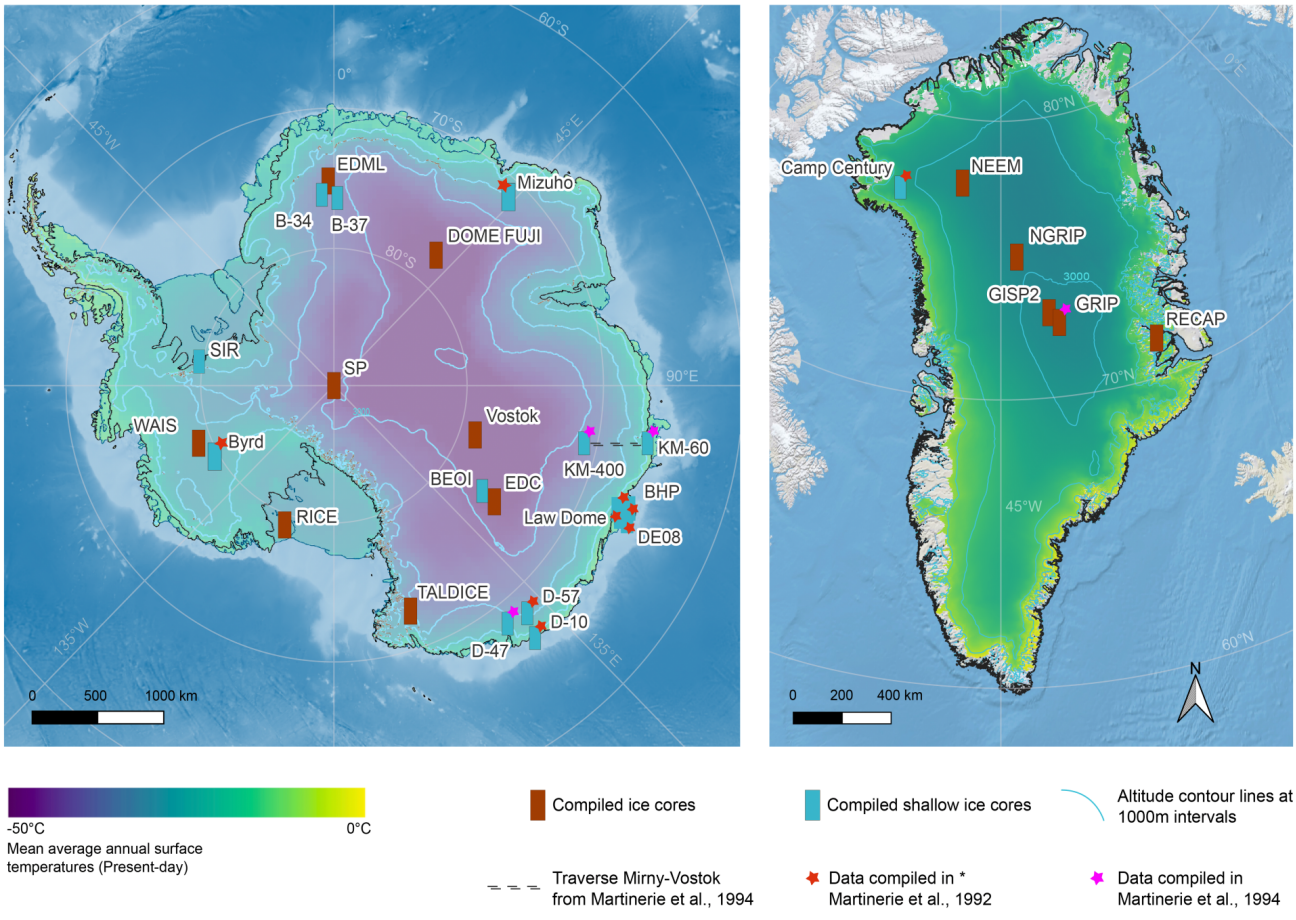

Figure 1. Maps of compiled TAC datasets in Antarctica and Greenland. *Sites compiled in Martinerie et al. (1992), analysed in later studies (Vostok, EDC, SP) are not labelled with a red star as newer datasets are used in this study (Table 2.). Maps generated using QGIS with the Quantarctica (Matsuoka et al., 2021) and QGreenland mapping environments (Moon et al., 2023; *Fisher et al., 2023)

The datasets compiled in Table 1 cover a wide range of environmental conditions, with accumulation rates ranging from 2.2 cm w.e./yr at Vostok to over 115 cm w.e./yr at DE08, reflecting the regional climatic difference between sites. Mean annual temperatures across the sites span from -57.3°C at DF on the Antarctic continental plateau to -13.5°C at BHF, in coastal Antarctica.

https://doi.org/10.5194/egusphere-2026-953
Preprint. Discussion started: 26 March 2026

Table 1: Overview of present-day site characteristics of datasets and corresponding Half Year Summer Insolation (HYSI) values computed for the past millennium.

Site	Latitude	Longitude	Elevation (m)	Mean Temp (°C)	Atm. Pressure (mbar)	Mean Acc. (w.e. cm/yr)	HYSI (W/m^2)
Ice cores compiled in this study							
DF[1]	77°19′S	39°42′E	3810	-57.3	596	2.6	374
EDC[2]	75°06′S	123°21′E	3233	-54.5	660	2.5	382
EDML[3]	75.00°S	0.07°E	2892	-44.6	676	6.4	382
GRIP[4]	72°35′N	37°34′W	3232	-31.6	665	23	376
NGRIP[5]	75°06′N	42°19′W	3090	-31.5	699	17.5	366
RECAP[6]	71°18'N	26°43'W	2340	-18	744	45.8	382
RICE[7]	79°36'S	161°71'W	550	-23.5	909	21	369
SP[8]	89°99'S	98°16'W	2835	-49	691	8	355
TALDICE[9]	72.78°S	159.07°E	2315	-41	721	8	391
Vostok[10]	78°28'S	106°50'E	3488	-56	632	2.2	371
WAIS[11]	79°28'S	112°05'W	1766	-31.1	778	20.2	367
SIR[12]	79°40'S	78°30'W	784	-26	893	13.5	369
Shallow ice cores compiled in this study							
BEOI[13]	75°21'S	122°28'E	3233	-54.5	645	2.4	382
B34[3]	75°00'S	00.07°E	2882	-44.6	676	6.5	382
B37[3]	75°00'S	00°40'E	2892	-44.6	676	6.4	382
Ice cores compiled in Martinerie et al., 1992							
BHJ[14]	65°95'S	113°10'E	130	-14	957	40	432
BHF[14]	66°10'S	111°00'E	360	-13.5	921	8	431
BHP[14]	66°15'S	111°15'E	610	-14	915	18	431
D-10[14]	66°40'S	139°55'E	270	-19	905	10 - 70	430
BHB[14]	66°20'S	111°30'E	773	-15.5	898	14	428
BHQ[14]	66°25'S	111°45'E	927	-17	876	6.5	429
DE08[14]	66°45'S	113°10'E	1250	-20	845	115	427
BHD[14]	66°45'S	112°50'E	1370	-21	834	68	427
Byrd[14]	80°00'S	120°00'W	1530	-28.7	806	16	367
CC[14]	77°10'N	61°10'W	1885	-24.9	793	34	359
D-57[14]	68°10'S	137°35'E	2053	-35.7	744	18	416
Mizuho[14]	70°40'S	44°15'E	2256	-34.5	732	7	403
Ice cores compiled in Martinerie et al., 1994							
KM-60[15]	67°05'S	93°19'E	*unpublished*	-20.8	*unpublished*	*unpublished*	424
KM-73[15]	67°12'S	93°17'E	*unpublished*	-21.1	*unpublished*	*unpublished*	423
KM-105[15]	67°26'S	93°23'E	*unpublished*	-24.5	*unpublished*	*unpublished*	422
KM-140[15]	67°45'S	93°39'E	*unpublished*	-27	*unpublished*	*unpublished*	420
KM-200[15]	68°15'S	94°05'E	*unpublished*	-30.5	*unpublished*	*unpublished*	416
KM-260[15]	68°46'S	94°28'E	*unpublished*	-33.5	*unpublished*	*unpublished*	414
KM-325[15]	69°18'S	95°01'E	*unpublished*	-37	*unpublished*	*unpublished*	410
KM-369[15]	69°44'S	95°30'E	*unpublished*	-38.8	*unpublished*	*unpublished*	409
KM-400[15]	69°57'S	95°37'E	*unpublished*	-39.9	*unpublished*	*unpublished*	405
D-47[15]	67°23'S	137°33'E	*unpublished*	-25.4	*unpublished*	*unpublished*	422

https://doi.org/10.5194/egusphere-2026-953
Preprint. Discussion started: 26 March 2026

EUROCORE[15]	72°21'N	37°33'E	*unpublished*	-32	*unpublished*	*unpublished*	377

References: [1] Oyabu et al. (2020), Buizert et al. (2021) (TAC) ; Watanabe et al. (1999) (Acc) ; Uemura et al. (2018) (Temp); Wang et al. (2023) (P), [2] Raynaud et al. (2007)(TAC) ; Cuffey and Paterson (2010) (Acc, Temp); Raynaud et al. (2007) (P), [3] this study (TAC) ; Cuffey and Paterson (2010) (Acc, Temp) ; Wang et al. (2023) (P), [4]Rasmussen et al. (2022) (Acc, Temp) ; Raynaud et al. (1997) (P, TAC), [5]Vinther et al. (2006) (Acc, Temp); Eicher et al. (2016)(P, TAC), [6]Vudayagiri et al. (2025) (TAC, Acc, Temp, P), [7]Lee et al. (2020) (TAC) Bertler et al. (2018) (Acc, Temp); Wang et al. (2023) (P), [8] Epifanio et al. (2023) (TAC) ; Severinghaus et al. (2001) (Acc, Temp); Martinerie et al. (1992) (P), [9] this study (TAC) ; Stenni et al. (2002) (Acc, Temp); Bock et al. (2017) (P), [10] Martinerie et al. (1994); Lipenkov et al. (2011) (TAC) ; Petit et al. (1999) (Acc, Temp) ; Martinerie et al. (1992)(P), [11]Buizert et al. (2021) (TAC) ; WAIS Divide Project Members (2013)(Acc, Temp); Wang et al. (2023) (P), [12] Wolff et al. (2024) (TAC) ; Mulvaney et al. (2021) (Acc, Temp) ; Wang et al. (2023) (P), [13] this study (TAC) ; Stenni et al. (2016) (Acc, Temp) ; Gautier et al. (2016) [14] Martinerie et al. (1992) (TAC, Acc, Temp, P), [15] Martinerie et al. (1994) (Temp). TAC, Acc and P are unpublished and will be published in a separate study.

2.2 Analytical methodologies for new TAC data

2.2.1 New TAC data measured at IGE

The new EDC TAC measurements covering the 440–800 ka interval (201 datapoints, measured between 2006 and 2007) were obtained using the barometric method at IGE as described in Lipenkov et al. (1995). These measurements extend the EDC TAC profile previously published by Raynaud et al. (2007) for the 0–440 ka interval, which was measured using the same experimental setup and calibration procedures. This method involves extracting air from ice samples by melting and refreezing under vacuum within a calibrated volume. The pressure and temperature of the extracted air are measured, allowing the calculation of TAC based on the ideal gas law (Equation 1.). Before calculating TAC, the water vapour pressure and the volume of refrozen ice in the cell are subtracted from the measured pressure and calibrated volume, respectively. The TAC is expressed in cm^3 of dry air at standard temperature and pressure (STP) per gram of ice, with an estimated accuracy of $\pm 1\%$ after correcting for cut-bubble effect (Eicher et al., 2016). A reproducibility of 1.3% was obtained from adjacent sample replicates, noting that horizontal variability from lens-shaped layering at low-accumulation sites like EDC contributes to this scatter. Measurements were independent of ice core storage duration (3 to 4 years post-drilling at -20°C), indicating negligible gas loss through molecular diffusion in ice.

2.2.2 New TAC data measured at the University of Bern

TAC data for the sites EDC (312 datapoints, measured between 2013 and 2023), EDML (12 datapoints, 2022), TALDICE (189 datapoints, 2012–2022), BEOI (5 datapoints, 2023), B34 (42 datapoints, 2012–2019), and B37 (28 datapoints, 2020–2023) were measured at the University of Bern using the melting air-extraction under vacuum technique described by Schmitt et al. (2014). This automated setup was originally developed for high-precision measurements of CH_4 and N_2O isotope and mixing ratios, but also allows for the determination of TAC as a by-product. Ice samples are slowly melted under vacuum with the released air efficiently removed from the headspace to minimize dissolution of the air in the liquid phase. The air is dried, collected, and expanded into a calibrated volume where pressure and temperature are recorded. TAC is then calculated using the ideal gas law and expressed in cm^3 STP per gram of ice, with corrections applied for gas retention in the meltwater and potential extraction losses (Schmitt et al., 2014). The accuracy of the Schmitt et al. (2014) method was assessed through several intercalibration exercises. Notably, it was compared with data obtained using the method of Lipenkov et al. (1995) on the EDC

https://doi.org/10.5194/egusphere-2026-953
Preprint. Discussion started: 26 March 2026

core (Raynaud et al., 2007), yielding a calibration factor uncertainty of 0.0005 $cm^3\ g^{-1}$ (0.5 mL kg^{-1}, approximately 0.5% for typical ice samples). The precision, estimated from vertical ice core replicates on TALDICE, is approximately 0.0006 $cm^3\ g^{-1}$ (∼0.6%) (Schmitt et al., 2014). In addition, consistent TAC values were confirmed for other previously measured ice cores, including NGRIP (Eicher et al., 2016), GRIP, and Vostok (Lipenkov et al., 1995).

For the EDML core specifically, most TAC values (198 datapoints) were obtained using the approach described in Eicher et al. (2016). In this method, air was extracted as a by-product of CH_4 and N_2O concentration measurements conducted at the University of Bern over many years. To ensure the consistency of absolute TAC values, the melt–refreeze method has been intercalibrated against the vacuum-melt dataset (Schmitt et al., 2011).

2.2.3 Corrections of the new TAC data

Air content measurements in polar ice cores require a correction for gas loss due to cut bubbles at the sample surface during preparation. Following the methodology of Martinerie et al. (1990), corrections were applied to account for air loss from bubbles intersected during sample cutting for all samples. The correction factor depends on the sample geometry, bubble size, and bubble shape, and was calculated using the statistical relationship linking the ratio of cut bubbles to total bubbles with the mean bubble size. For cubic ice samples with approximately 3 cm edge length, corrections typically ranged from ∼ 1 to 10% of the measured air content value with larger corrections for shallow ice above ∼ 200 m depth. Bubble characteristics (size and shape) were determined from thin section analysis, and the correction was applied using the appropriate equations for spherical or cylindrical bubble geometries as described in Martinerie et al. (1990).

2.3 Criteria for exclusion and segregation of TAC datasets

The TAC datasets are segregated into two groups used for different types of analyses. Temporal-scale analyses are performed on millennial- and orbital scales. Datasets covering more than 40 ka are used to assess the TAC signal at orbital timescales in order to cover both glacial and interglacial values. High-resolution data is used to investigate the TAC variability at millennial scales. Low or high resolution data covering the last millennia is used for spatial-scale analyses (see section 3.). Spatial-scale analyses require careful assessment of discrepancies between datasets in terms of measurement techniques and applied corrections. For detailed descriptions of the analytical methods used for published TAC datasets, we refer the reader to the original publications listed in Table 1. Sites with documented recent melting events are excluded from our study. This applies to the RICE site, also excluded due to the uncertainties in the cut-bubble effect corrections applied (Lee et al., 2020). For the RECAP site, we used a TAC value set to a present-day value with no melting determined by Vudayagiri et al. (2025) (Table A1.). Intervals with data gaps exceeding 10% of their total length are excluded from the temporal analysis to avoid misinterpreting gaps as changes in temporal resolution. This exclusion criterion applies only to the DF dataset.

https://doi.org/10.5194/egusphere-2026-953
Preprint. Discussion started: 26 March 2026

2.4 Investigated climate parameters

Ice core datasets for temporal-scale analysis are detailed in Table 2, including TAC methods, chronologies, and surface parameters (e.g. simulated summer temperatures, calculated summer insolation, reconstructed annual temperatures and accumulation rates). Raw datasets are plotted in Fig. A1. Spatial-scale analysis examines recent TAC with atmospheric pressure, elevation, temperature, accumulation, and insolation (HYSI), with site data in Table 1.

Site	TAC (datapoints, interval (ka), method)	Dating Model	Temperature (interval (ka), method)	Accumulation (interval (ka), method)
DF	80[1], [2-156], subproduct[1] + 95[2], [3-42], direct[3]+ subproduct[1]	DF2021[4]	[0-208], Water Stable Isotope[5]	[0-208], Water Stable Isotope + model[4]
EDC	417[6], [2-800], direct[3]	AICC2023[7]	[0-806], Water Stable Isotope[8]	[0-809], Modelled AICC2023[7]
EDML	198[9], [11-56], subproduct[10]	AICC2023[7]	[1-140], Water Stable Isotope[11]	[0-145], Modelled AICC2023[7]
GRIP	222[12], [0-53], direct[3]	GICC05[13]	[0-100], Water Stable Isotope available[14]	[0-248], Annual-layer counting[15]
NGRIP	1560[16], [11-122], subproduct[10,16]	GICC05[13]	[9-122], δ^{15}N + firn modelling [17]	[9-122], Layer-counting + diffusion[17]
RECAP	521[18], [0-120], direct[3]+ subproduct[19]	GICC05[13]	-	-
RICE	418[20], [0-80], subproduct[21]	RICE17[22]	-	[0-2.7], Annual-layer counting[22]
SP	1061[23], [1-54], subproduct[19]	SP19[24,25]	[1-53], Inverse method[26]	[1-53], Inverse method[26]
TALDICE	189[27], [0-120], subproduct[10]	AICC2023[7]	[0-40], δ^{15}N + borehole thermometry[28]	[0-490], Modelled AICC2023[7]
Vostok	152[29], [4-163], direct[30] + 156[31], [163-408], direct[3]	AICC2023[7]	[0-422], Water Stable Isotope[8]	[0-408], Modelled AICC2023[7]
WAIS	1189[2], [0-50], subproduct[21]	WD2014[32]	[0-67], Water Stable Isotope[33]	[0-68], Layer counting + inverse method[34]

Table 2. Overview of investigated surface parameters for temporal analyses.

References: [1] Oyabu et al. (2020); [2] Buizert et al. (2021); [3] Lipenkov et al. (1995); [4] Oyabu et al. (2022); [5] Uemura et al. (2018); [6] Raynaud et al. (2007); this study; [7] Bouchet et al. (2023); [8] Jouzel et al. (2007); [9] this study; [10] Schmitt et al. (2014); [11] Stenni et al. (2010); [12] Raynaud et al. (1997); [13] Rasmussen et al. (2022); [14] Johnsen (2003); [15] Hammer and Dahl-Jensen (1999); [16] Eicher et al. (2016); [17] Kindler et al. (2014); [18] Blunier (2024); Vudayagiri et al. (2025); [19] Mischler et al. (2009); Fegyveresi (2015); [20] Lee et al. (2020); [21] Mitchell et al. (2015); [22] Winstrup et al. (2019); [23] Epifanio et al. (2023); [24] Winski et al. (2019); [25] Epifanio et al. (2020); [26] Kahle et al. (2021); [27] this study; [28] Buizert et al. (2021); [29] Martinerie et al. (1994); [30] Raynaud et al. (1982); [31] Lipenkov et al. (2011); [32] Buizert et al. (2015); [33] Cuffey (2017); [34] Fudge et al. (2016)

We use the Half Year Summer Insolation (HYSI) index (Raynaud et al., 2024), which represents the average insolation over the astronomical summer half-year, accounting for both total energy received and season length. The astronomical summer half-year in the SH, corresponding to the astronomical winter half-year in the NH, is defined as the time from the fall equinox (September) to the spring (March) equinox (Berger et al., 1993, 2010, 2024). The computation of this insolation index accounts for orbital parameters (e.g. eccentricity, obliquity, and precession) following Berger (1978). This made HYSI a more physically consistent orbital dating tool, strongly anti-correlated with TAC and correlated with modelled summer surface temperatures (Raynaud et al., 2024). We computed these HYSI for all compiled sites covering the same time interval as the sites' TAC datasets (Table 2). Mean computed HYSI values over the past millennia are shown in Table 1 for each site and are used for the spatial-scale analysis.

https://doi.org/10.5194/egusphere-2026-953
Preprint. Discussion started: 26 March 2026

For temporal analysis at orbital timescales, we use published reconstructions of annual surface temperature and accumulation rates (Table 2). Temperature reconstructions are primarily derived from water stable isotopes (DF, EDC, EDML, Vostok, WAIS), with additional methods including δ^{15}N and firn modeling (NGRIP), borehole thermometry (TALDICE), or inverse methods (SP). Accumulation reconstructions rely on annual-layer counting (GRIP, RICE, WAIS), modeled chronologies (EDC, EDML, TALDICE, Vostok from AICC2023), or combinations of layer-counting and diffusion/inverse methods (NGRIP, SP, WAIS). For spatial-scale analysis, we compile present-day field measurements of atmospheric pressure, elevation, mean annual temperature, and annual accumulation rate for each site (Table 1).

In the study by Raynaud et al. (2024), the LOVECLIM 1.3 model (Yin et al., 2021) is used to simulate summer surface air temperatures by incorporating variations in orbital parameters, greenhouse gas concentrations, and ice sheet configurations. LOVECLIM 1.3 is an Earth system model of intermediate complexity (EMIC) with coupled atmosphere (ECBilt), ocean and sea ice (CLIO), and terrestrial biosphere (VECODE) components. The model has been shown to reproduce the spatial changes and magnitudes of surface temperatures over Antarctica. These simulated temperatures showed good agreement with TAC records at the EDC site, highlighting the model's reliability in capturing orbital-scale variability (Raynaud et al., 2024). Building on this study, we use outputs from the same model to explore the relationship between local summer insolation, summer temperatures, and TAC at GRIP, SP, NGRIP, EDC, Vostok, TALDICE and RECAP sites extending the analysis beyond EDC to assess regional patterns.

2.5 Age scale considerations and temperature approximations

The interpretation of TAC variations, in particular at temporal-scale, requires a careful consideration of age scales (Edwards and Epifanio, 2025). Different physical processes affecting TAC operate on different timescales: some are recorded at discrete points in time (e.g., ice age or gas age), while others represent time-integrated effects over the full densification period. In particular, we can consider three type of age scales that are relevant when studying TAC changes and that should be specified depending on which mechanism is being investigated:

- **Ice age scale:** Summer insolation (HYSI) affects near-surface snow metamorphism, a process recorded in the ice matrix during early densification. Therefore, the investigation of the TAC-HYSI relationship should rely on the TAC record being displayed on the ice age scale (Raynaud et al., 2024).
- **Gas age scale:** Temperature effects on air density at close-off via the ideal gas law require TAC on the gas age scale. Transient effects during abrupt climate events (e.g., D-O events), where rapid accumulation increases cause enhanced overburden pressure and dynamic compression of the firn at close-off depth (Eicher et al., 2016), operate on a very short timescale, as the weight of new snow is directly transmitted to the close-off depth. Note that heat diffusion from surface to close-off depth introduces an additional time lag, though this is generally small compared to ice-gas age differences at low accumulation sites.
- **"Densification age scale"**: Temperature and accumulation effects on pore volume (V_c) integrate conditions over the full densification period (for example at EDC: ∼1.6 kyr during warm interglacials, up to ∼4.6 kyr during the last glacial

https://doi.org/10.5194/egusphere-2026-953
Preprint. Discussion started: 26 March 2026

maximum). This integration depends on the depth sensitivity of temperature and accumulation to firn structure (Raynaud et al., 2007) and could be approximated as a "mid-age scale" (in between ice and gas ages), though this represents a simplification of a more complex, non-discrete integration period. The relevant timescales differ between temperature (complicated by heat diffusion) and accumulation (which modulates the duration available for densification).

In this study, we approximate that the surface temperature T_s is equal to T_c, $T_s = T_c$, the close-off temperature. Hence, we use mean annual surface temperature reconstructions from water stable isotopes, following Martinerie et al. (1992); Raynaud et al. (2007). This simplification is justified for two reasons. First, for spatial analysis, climate has remained relatively stable over firn residence times (ranging from a few decades at high-accumulation sites to several thousand years at low-accumulation sites under glacial conditions). Second, for temporal analysis at orbital timescales, age scale uncertainties of a few thousand years have minimal impact on correlation structures. We primarily focus on temperature effects on pore volume (V_c) and correlate both TAC and temperature on the ice age scale (Table A2). This choice reflects the fact that temperature reconstructions from water stable isotopes are given on the ice age scale and is formally appropriate only for HYSI-TAC correlations. However, it represents an approximation for the temperature-V_c relationship, which should strictly use a densification integrated age scale to account for heat conduction through the firn (∼100-year lag from surface to close-off depth). Also, we note that the present-day spatial relationship between V_c and mean annual surface temperature established by Martinerie et al. (1992) is not fully understood in terms of its temporal applicability, given the inverse relationship between V_c and summer temperature identified at orbital timescales (Raynaud et al., 2024) and the age scale approximations. To assess the sensitivity of our results to age scale choice, we performed correlations with TAC on the ice age scale (Table A2) and gas age scale (Table A3).

While firn heat diffusion modelling (Goujon et al., 2003) would provide more accurate close-off temperatures and enable rigorous "densification integrated" age-scale analysis, reconstructing T_c for all compiled sites is beyond the scope of this study.

2.6 Statistical analyses

The investigation of the relationship between TAC and several surface parameters was conducted using a combination of data resampling, low-pass filtering and linear regression analysis. The different datasets (e.g. TAC and environmental variables) are interpolated onto a time grid with a step of 1 ka using a linear interpolation and averaging. To isolate orbital-scale variations, we applied a Finite Impulse Response (FIR) low-pass filter to the interpolated data. This approach follows the method of Kawamura et al. (2007), who advises a Kaiser-window FIR filter with a 16.7 kyr cut-off period to retain precessional-scale variations and eliminate high-frequency noise below 10 kyr. The FIR filter was implemented bidirectionally to prevent phase distortion, in order to keep peak positions in the filtered signal aligned with the original time series. By applying the same filter parameters across all datasets, short-term variability is removed in a uniform manner, allowing for a direct comparison of long-term trends across ice core records of varying temporal extents (from 50 ka to 800 ka).

Linear regression analyses were performed using ordinary least squares (OLS), which assumes negligible uncertainty in the independent variable (Fig. A4.). While more rigorous approaches accounting for uncertainties in both variables exist (York et al., 2004), the use of OLS is justified at orbital timescales where signal amplitudes exceed measurement uncertainties, and is

https://doi.org/10.5194/egusphere-2026-953
Preprint. Discussion started: 26 March 2026

consistent with previous TAC studies (Raynaud et al., 2007; Lipenkov et al., 2011). Linear regression analyses were performed on unfiltered and filtered datasets to quantify the degree of correlation between TAC and each parameter. Regression slopes, R and R^2 are calculated, along with p-values to assess the robustness of the observed relationships. Moreover, to account for data gaps in different time series such as DF and ensure a robust assessment of the relationship between TAC and environmental parameters across different periods, we computed a weighted global coefficient of determination (R^2) by combining the results obtained from two distinct time intervals of different resolution separated by a data gap.

3 Results

3.1 The EDC TAC records

Building upon the EDC TAC profile published by Raynaud et al. (2007), which used samples from EDC96 (115-783 m) and EDC99 (below 783 m) cores down to 2798 m depth, we extended the record down to 800 ka through measurements performed in 2006-2007 at IGE (Fig. 2.a.). We analysed 396 depth levels on the EDC99 core between 2798 and 3254 m. Here, we only show data down to 3190 m since flow disturbances affect the bottom 60 m of the core (Jouzel et al., 2007). This new dataset has an average temporal resolution of 2.04 ka for the entire record. The statistical properties of the TAC values across the entire 800 ka span indicate a mean of 0.0911 $cm^3\ g^{-1}$ with a standard deviation of 0.0024 $cm^3\ g^{-1}$ and a range of 0.0131 $cm^3\ g^{-1}$ (minimum: 0.0850, maximum: 0.0981). The variance of $5.68\times10^{-6}(cm^3\ g^{-1})^2$ shows a relatively low dispersion around the mean, supporting reproducibility of the measurements throughout the record. Overall, the new TAC signal exhibits orbital-scale related changes, not directly correlated with the δD temperature proxy, but displaying a relationship with the HYSI index (Fig. 2.d. and e.). Continuous wavelet transform (CWT) analysis of the IGE EDC dataset reveals distinct orbital signatures across different time intervals (Fig. A3.). The complete record (0-800 ka, n=392) exhibits dominant cyclicities at about 100 kyr and 41 kyr. The 100-kyr periodicity is characteristic of glacial-interglacial cycles and primarily reflects the imprint of ice sheet dynamics rather than direct eccentricity forcing. The 41 kyr signal is related to obliquity and is consistent with local summer insolation control on snow metamorphism (Raynaud et al., 2024), though we cannot exclude contributions from climate teleconnections (Raymo and Nisancioglu, 2003). The recent interval (0-440 ka, n=213) investigated in Raynaud et al. (2007) shows strongest obliquity signals with secondary 100 kyr variability, while the older interval (440-800 ka, n=179) displays 100 kyr dominance with precession cycles at 23-24 kyr.

An independent EDC dataset was also produced at the University of Bern (Fig. 2.b.) covering the 21-660 ka time interval. The Bern dataset comprises 349 data points and shows a similar mean TAC of 0.0920 $cm^3.g^{-1}$, with a variance of $4.21\times10^{-6}(cm^3\ g^{-1})^2$ and with an average temporal spacing of 1.84 ka across the full interval. In the interval between 200–400 ka, the Bern TAC data has a mean spacing of 0.90 ka compared to 2.52 ka over the same interval for the IGE EDC dataset. Despite different analytical approaches, both datasets show strong agreement on the highest resolution interval (Fig. 2.c.). These observations are consistent with the intercalibration performed between the Bern and IGE methods on the EDC ice core (Schmitt et al., 2014; Raynaud et al., 2007), which constrained the calibration uncertainty to 0.0005 $cm^3\ g^{-1}$ ($\sim$0.5%), and with previous comparisons between Greenland ice cores (Eicher et al., 2016). The new high-resolution Bern TAC record over

https://doi.org/10.5194/egusphere-2026-953
Preprint. Discussion started: 26 March 2026

the 427-224 ka interval reveals interesting millennial-scale TAC changes superimposed onto the orbital-scale variations signal which are further investigated in section 3.3.1.

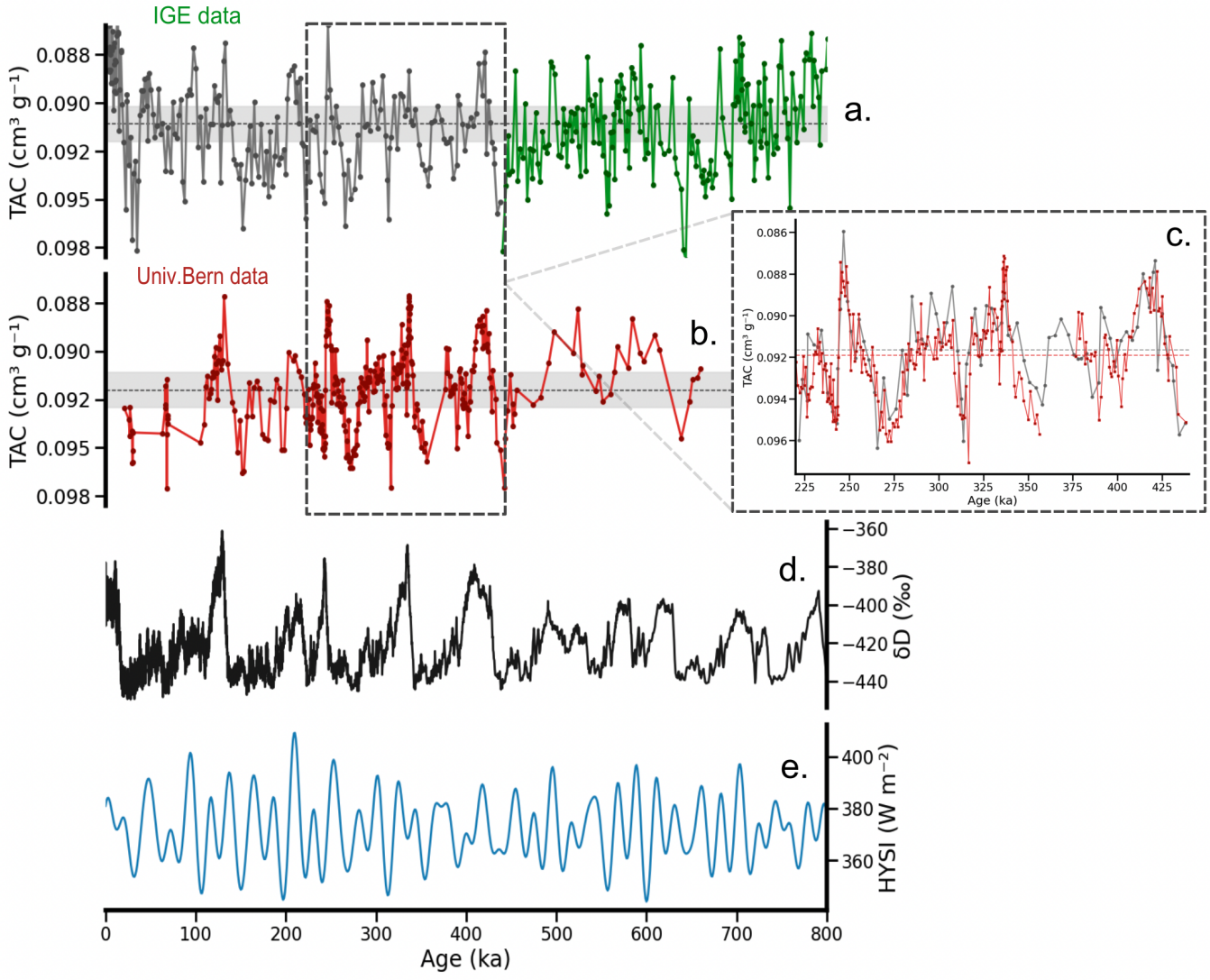

Figure 2. TAC profile of the EDC ice core. **a.** TAC measured at IGE with the Lipenkov et al., 1995 method. Published data from Raynaud et al. (2007) in grey, new data in green. **b.** TAC measured at the University of Bern with Schmitt et al., 2014 method (in red). The dashed black line in a. and b. represents the mean TAC value over the past 800 ka, associated with the typical 1% analytical uncertainty range in grey. **c.** Superimposed EDC TAC records from EDC IGE and the University of Bern between 220 and 430 ka. Corresponding mean TAC values are displayed in dashed horizontal lines. **d.** EDC δD record (black, Jouzel et al. (2007). **e.** EDC Half Year Summer Insolation (HYSI) index. TAC and δD data are displayed on the AICC2023 ice age scale. TAC is shown on a reversed scale. (Bouchet et al., 2023).

https://doi.org/10.5194/egusphere-2026-953
Preprint. Discussion started: 26 March 2026

3.2 TALDICE, EDML and shallow ice core records

New TAC data on TALDICE, EDML and three shallow ice cores (B34 , B37 and BEOI) were also measured at the University of Bern. The TALDICE record (Fig. 3.) spans the last 152 ka and exhibits TAC values between 0.094 and 0.107 $cm^3\ g^{-1}$ (mean = 0.103, σ = 0.003, n=189), with an average resolution of 0.8 ka. The new TALDICE TAC record displays orbital-scale variations that reflect the combined influences of summer insolation (HYSI) and temperature (δD) (Fig. 3). These changes can notably be seen over the 0-90 ka time interval covered with higher sampling resolution. The EDML core (Fig. A2.a.) covers the 10-56 ka interval, with TAC values ranging from 0.082 to 0.105 $cm^3\ g^{-1}$ (σ = 0.004, n=198). Depths range from 686 to 1617 m, and temporal resolution varies: 0.11 ka between 10-30 ka, a 5.4 ka data gap, and 1.3 ka from 35-55 ka, after 90 ka, it remains very low.

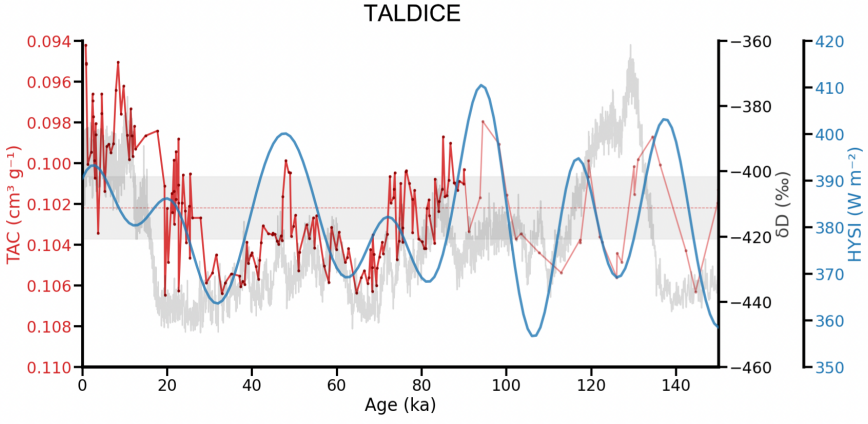

Figure 3. The TALDICE TAC record displayed on the AICC2023 ice age scale (Bouchet et al., 2023) and measured at the University of Bern with Schmitt et al. (2014) method (in red). TAC is shown on a reversed scale. The dashed red line represents the mean TAC value over TAC dataset associated with the typical 1.5% analytical uncertainty range in grey. The TALDICE-TAC dataset is superimposed with the corresponding Half Year Summer Insolation (HYSI) index (in blue) and the EDC δD record (in grey, Jouzel et al. (2007))

TAC measurements on the shallow cores B34 (179.18-180.94 m, n=42), B37 (106.43-114.57 m, n=28), and BEOI (131.37-131.93 m, n=5) were performed just below the close-off depth ((Fig. A2.b.c.d.), yielding mean values of 0.092, 0.088, and 0.086 $cm^3\ g^{-1}$ respectively, with low standard deviations (0.0008, 0.001, and 0.001 $cm^3\ g^{-1}$). The shallow cores demonstrate good measurement precision and internal consistency within each core. Notably, despite their geographic proximity (and similar insolation), cores B34 and B37 show a significant difference in their mean TAC values (0.092 vs 0.088 $cm^3\ g^{-1}$), highlighting the sensitivity of TAC to local surface conditions (accumulation rate, temperature, wind).

https://doi.org/10.5194/egusphere-2026-953
Preprint. Discussion started: 26 March 2026

3.3 Temporal-scale variations of TAC

Here, we conduct linear regression analyses between TAC records from the different compiled ice core sites and their corresponding local climatic conditions to investigate their link at a temporal scale (Fig. 4.).

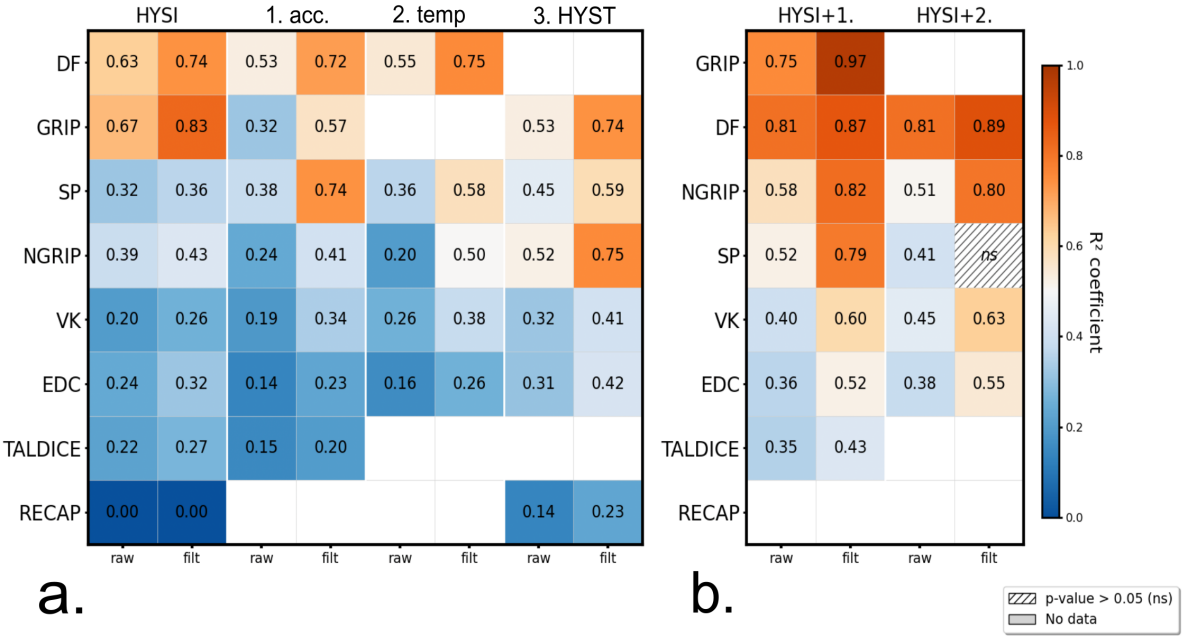

Figure 4. Heatmap of R^2 derived from linear regression analyses between TAC and HYSI, 1. Reconstructed annual accumulation rates (acc.), 2. Reconstructed annual temperatures (temp.) and 3. Simulated half year temperatures (HYST). Sites are sorted from top to bottom by highest mean of R^2. Analyses conducted for **a.** simple linear regression and **b.** multiple regressions analyses of TAC vs HYSI + surface parameter. *raw: Raw datasets*; *filt: filtered data using a 16.7-kyr low-pass FIR filter.* All data was processed on their corresponding ice age scale (Table 2.)

First we examine the link between TAC and local HYSI across different sites. Regression equations, r and R^2 are compiled in Table A2. The strongest correlations are found at DF and GRIP with R^2 values above 0.5 for both raw and filtered records (DF: R^2 = 0.63 raw, 0.74 filtered; GRIP: R^2 = 0.67 raw, 0.83 filtered). In contrast, other Antarctic sites show weaker correlations, with R^2 below 0.3 for raw data (EDC: R^2 = 0.24 raw, 0.32 filtered; Vostok: R^2 = 0.20 raw, 0.26 filtered), while RECAP shows no correlation. For accumulation rates, we find the strongest correlation at SP and DF (SP: R^2 = 0.38 raw, 0.74 filtered; DF: R^2 = 0.53 raw, 0.72 filtered), while showing weaker correlations elsewhere (NGRIP: R^2 = 0.24 raw, 0.41 filtered; Vostok: R^2 = 0.19 raw, 0.34 filtered). Reconstructed temperatures show the strongest correlations with TAC at DF (R^2 = 0.55 raw, 0.75 filtered) and more moderate correlations at other sites. Simulated half-year summer temperatures, show significant correlation at NGRIP, GRIP and SP (NGRIP: R^2 = 0.52 raw, 0.75 filtered; GRIP: R^2 = 0.53 raw, 0.74 filtered; SP: R^2 = 0.45 raw, 0.59 filtered), but remain less correlated at EDC (R^2 = 0.31 raw, 0.42 filtered) and Vostok (R^2 = 0.32 raw, 0.41 filtered).

https://doi.org/10.5194/egusphere-2026-953
Preprint. Discussion started: 26 March 2026

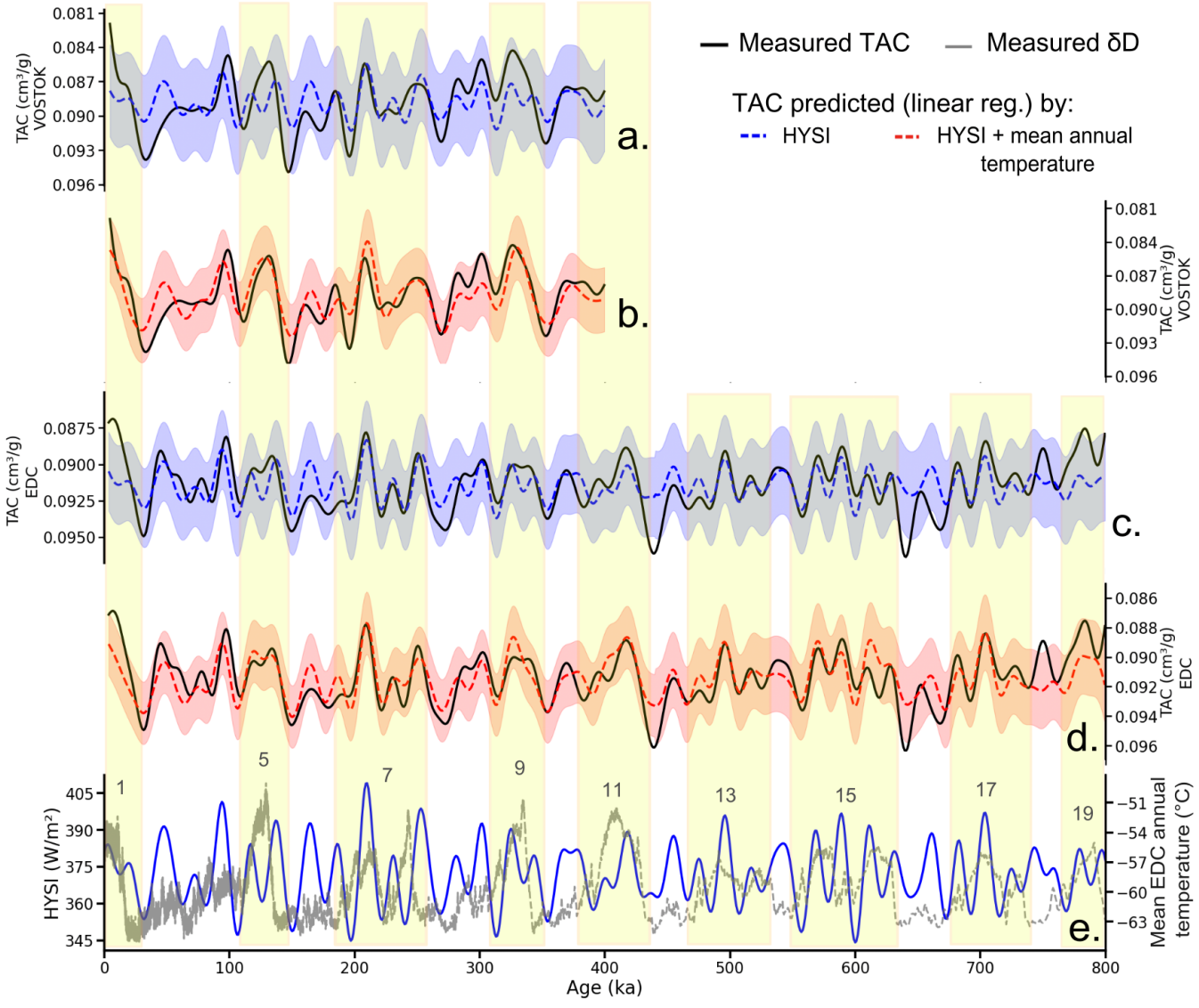

Figure 5. Comparison of measured and predicted TAC at two Antarctic ice core sites. **(a.-b.)** Vostok site: TAC predicted using **a.** simple linear regression with HYSI only **(R^2 = 0.26)** and **b.** multiple linear regression with HYSI + annual temperature **(R^2 = 0.63)**. **(c.-d.)** EDC site: TAC predicted using **c.** simple linear regression with HYSI only **(R^2 = 0.32)** and **d.** multiple linear regression with HYSI + annual temperature **(R^2 = 0.55)**. Black lines in panels **(a.-d.)** show measured TAC data after applying a 10 kyr filter to remove millennial-scale variability. Annual Temperatures reconstructions are from Jouzel et al. (2007). **e.** represents the reconstructed temperature EDC dataset plotted in gray (Jouzel et al., 2007) superimposed with the EDC Half Year Summer Insolation (HYSI) index in blue. Blue and red bands represent the 95% Prediction interval (Predicted value ± MSE). Yellow boxes highlight significant visual improvements of the predicted signal. Interglacials are numbered from MISs 1 to 19 (Past Interglacials Working Group of PAGES, 2016). Both TAC and predictor variables were filtered using a 16.7-kyr low-pass FIR filter to capture orbital-scale variations. All plots are displayed on the AICC2023 ice age scale (Bouchet et al., 2023). TAC is shown on a reversed scale.

https://doi.org/10.5194/egusphere-2026-953
Preprint. Discussion started: 26 March 2026

Low-resolution sites (TALDICE, RECAP) show consistently poor correlations across all parameters (Fig. 4.), emphasizing the critical importance of high temporal resolution for capturing TAC-climate relationships. Across all parameters, filtering can improve correlations by removing high-frequency variability and noise, isolating the orbital-scale signal. We also note that temperature regression slopes (Table A2) are consistent with the empirical V_c-T relationship of Martinerie et al. (1992) at Vostok but approximately half at EDC, suggesting site-specific differences in TAC controls.

To account for the combined influence of insolation and surface climate parameters, we performed multiple regression analyses using HYSI together with individual local surface parameters (Fig. 4.b.). This approach improved the explained variance of the different regressions, demonstrating the combined effects of orbital forcing and surface annual temperature or accumulation responses. For instance, at DF, the combination of HYSI with accumulation rates raised R^2 values to 0.81 for raw data and 0.87 for filtered data. Even sites with initially weak correlations showed improvements: EDC increased from $R^2 = 0.24$ (HYSI alone) to 0.52 with accumulation, and Vostok improved from $R^2 = 0.20$ to 0.60 with temperature (via the temperature effect on pore volume V_c, see section 2.5). Combinations with simulated half-year summer temperatures are not significant due to inherent correlations between these temperature simulations and HYSI, as half-year temperature is primarily determined by local summer insolation (Raynaud et al., 2024). They are therefore not shown nor analysed in the multi-regression analyses results.

To further investigate how combining the influence of the insolation and the temperature (Fig. 5.e.) could enable to better predict the TAC changes, we examine in detail the Vostok and EDC records (Fig. 5.). We compare measured TAC (black curves) with TAC predicted by a simple regression using either HYSI alone (blue curves) or HYSI combined with reconstructed annual temperature (red curves). The regression equations are detailed in Table A4. This comparison enables to highlight the time intervals when the combined influence of both parameters is important. At Vostok, TAC predicted by a simple regression with HYSI alone ($R^2 = 0.26$; Fig. 5.a., blue curve) failed to capture the full amplitude of TAC variations during deglaciations, when major shifts in surface climate conditions occur. When HYSI was combined with temperature in a multiple regression model ($R^2 = 0.63$; Fig. 5.b., red curve), the predicted TAC closely matched observed variations, particularly during Marine Isotope Stages (MIS) 1, 5, 7, and 9 (Fig. 5.b.). Similar improvements are observed at EDC, where the R^2 increases from 0.32 (HYSI only, Fig. 5.c.) to 0.55 (HYSI + temperature, Fig. 5.d.). It is worth noting that lower TAC values between 25–40 ka in Vostok may reflect gas loss from poor ice quality in the brittle zone.

3.3.1 Millennial-scale TAC changes in the EDC ice core

High-resolution TAC measurements from EDC measured at Bern University revealed significant millennial-scale variations superimposed onto the HYSI orbital signal (Fig. 6.).

Panel (a) shows measured TAC data (blue) alongside HYSI (gray), displaying clear orbital-scale covariation. Beyond this orbital variability, residual analysis obtained by removing the HYSI-predicted component from the raw TAC signal (Fig. 6.b.) reveals positive and negative anomalies with amplitudes reaching ± 0.005 cm^3/g. The most prominent millennial-scale TAC

https://doi.org/10.5194/egusphere-2026-953
Preprint. Discussion started: 26 March 2026

peaks occur during intervals centred around 240 ka and 335 ka (highlighted in yellow), coinciding with the large Antarctic warmings during the glacial terminations TIII and TIV and associated with a δD increase of about 60 ‰ in 5 ka (Fig. 6.c., e.).

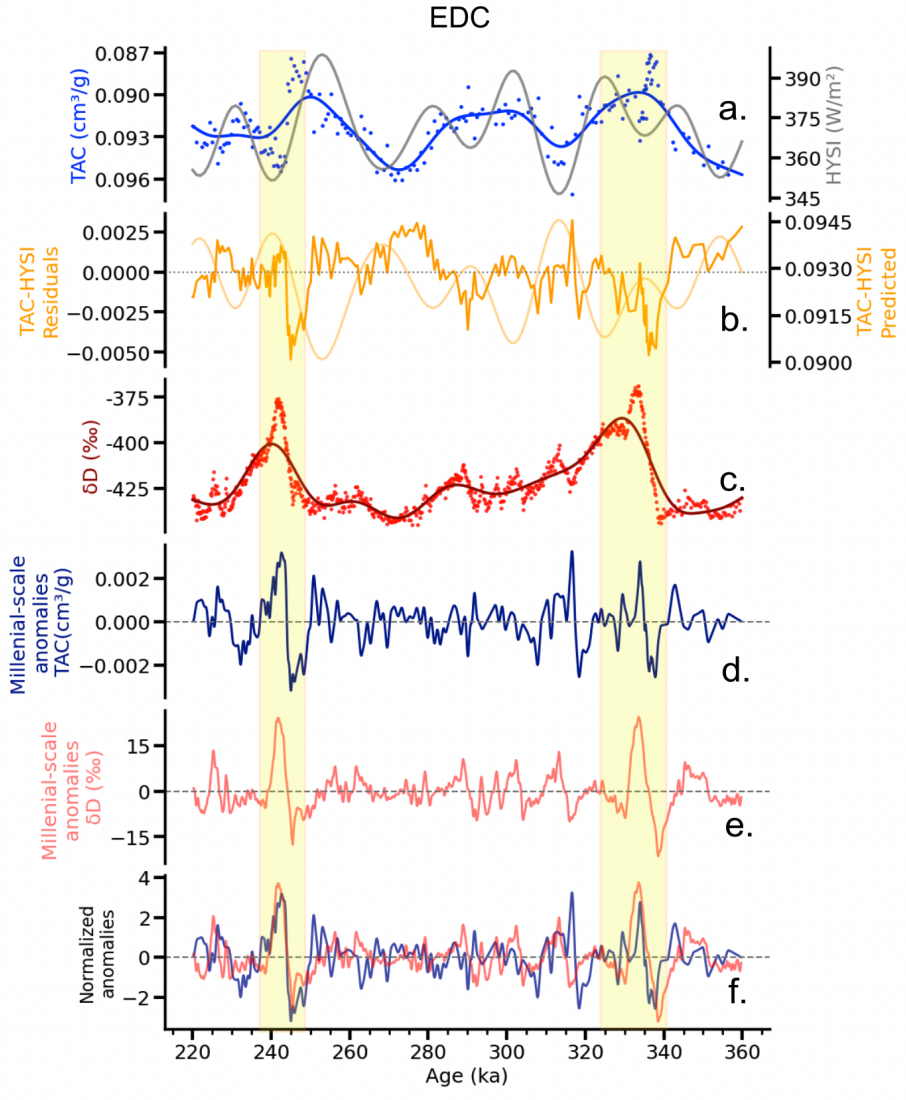

Figure 6. Investigation of millennial-scale TAC changes at EDC site. **a.** TAC signal raw (data mesured at University of Bern) and filtered, superimposed onto the HYSI index. **b.** TAC residuals from the linear regression TAC vs HYSI superimposed to the TAC signal exclusively predicted by the linear relationship of TAC vs HYSI. **c.** δD raw superimposed (Jouzel et al., 2007) to δD filtered signal. **d.** TAC raw – TAC filtered). **e.** Millennial-scale δD anomalies (δD raw – δD filtered). **f.** Normalized millennial-scale anomalies (TAC and δD). Yellow boxes represent time intervals of strong millennial-scale TAC variations parallel to δD large changes. All variables are filtered using a 16.7-kyr low-pass FIR filter. All plots are displayed on the AICC2023 ice age scale (Bouchet et al., 2023). TAC is shown on a reversed scale.

https://doi.org/10.5194/egusphere-2026-953
Preprint. Discussion started: 26 March 2026

Millennial-scale TAC anomalies obtained through high-pass filtering (Fig. 6.d.) confirm the presence of rapid variations with amplitudes of ± 0.003 cm^3/g (representing about 30% of the total TAC signal) and show synchronized patterns with δD anomalies reaching ± 10 ‰, particularly during these deglaciation periods (Fig. 6.e.). The normalized superposition of millennial-scale anomalies (Fig. 6.f.) confirm that TAC and δD are synchronous with minimal time lag (on the centennial order) around 240 and 330 ka, contrasting with the larger temporal offset observed between TAC and HYSI peaks around 240 ka. Beyond the two major highlighted events, smaller-scale variations can be seen throughout the record, with TAC residuals showing both positive and negative excursions. It should be noted that time lags or leads can change regarding the strength of the filter applied (here 16.7 kyr low-pass FIR filter).

4 Discussion

4.1 Spatial-scale of recent TAC and pore volume

The spatial-scale analysis of the relationship of TAC and pore volume (V_c) with surface parameters (e.g. elevation, atmospheric pressure, temperature, wind) is an approach used in Martinerie et al. (1992, 1994) and Delmotte et al. (1999). We updated this analysis using an expanded dataset with additional sites and surface parameters (e.g. HYSI) and calculated mean TAC for recent periods (Table A1.) from stable values below close-off depth according to these previous studies. The spatial-scale investigation of TAC was conducted across atmospheric pressure ranges of 632-957 mbar and elevations of 130-3233 m. We observe strong TAC-pressure correlations ($R^2 = 0.96$), consistent with the ideal gas law (equation 1.)and comparable to Martinerie et al. (1992) ($R^2 = 0.98$) across our expanded dataset (Fig. 7.a.). Since recent TAC values primarily reflect the very large elevation range of study sites, we focus our spatial-scale analysis on pore volume (V_c) calculated from TAC using equation (1). TAC and V_c values are provided in Table A1.

To quantify the temperature dependence of pore volume, we performed a linear regression between our calculated V_c values and close-off temperatures T_c, extrapolated to be the present-day surface temperatures following Martinerie et al. (1992). This empirical relationship ($R^2 = 0.86$, Fig. 7.b.) closely matches Martinerie et al. (1992) and Delmotte et al. (1999) findings and their equation used in subsequent V_c studies (Raynaud et al., 2007; Eicher et al., 2016).

We also examined V_c correlations with the logarithm of accumulation rates, showing moderate correlation for all sites: $R^2 = 0.55$ (Fig. 7.c.). However, the accumulation-based correlation must be interpreted cautiously given the large spatial variability in accumulation patterns and the known temperature-accumulation coupling (Martinerie et al., 1992).

Building on established temporal relationships between TAC and insolation (Raynaud et al., 2007, 2024), we investigate for the first time the spatial correlation between V_c and HYSI. The V_c - HYSI relationship (Fig. 7.d.) shows a R^2 of 0.44 when all studied ice core sites are considered. However, a R^2 of 0.89 is found when the analysis considers only sites located in East Antarctica (Fig. 7.e.). This suggests that HYSI influences TAC values at spatial scale. In contrast, the linear regression including only Greenland and West Antarctic sites (Non-EAIS) suggest no significant link between TAC and HYSI (not shown here). These results suggest a marked regional heterogeneity in V_c - climate relationships. EAIS sites V_c values are

https://doi.org/10.5194/egusphere-2026-953
Preprint. Discussion started: 26 March 2026

closely correlated to insolation and Non-EAIS sites V_c values are controlled by combined surface climate processes including insolation, temperature and accumulation rates. It should be noted that some coastal sites from the Law Dome area could have experienced summer melting (Martinerie et al., 1992), they should therefore be considered carefully and potentially be source of uncertainties.

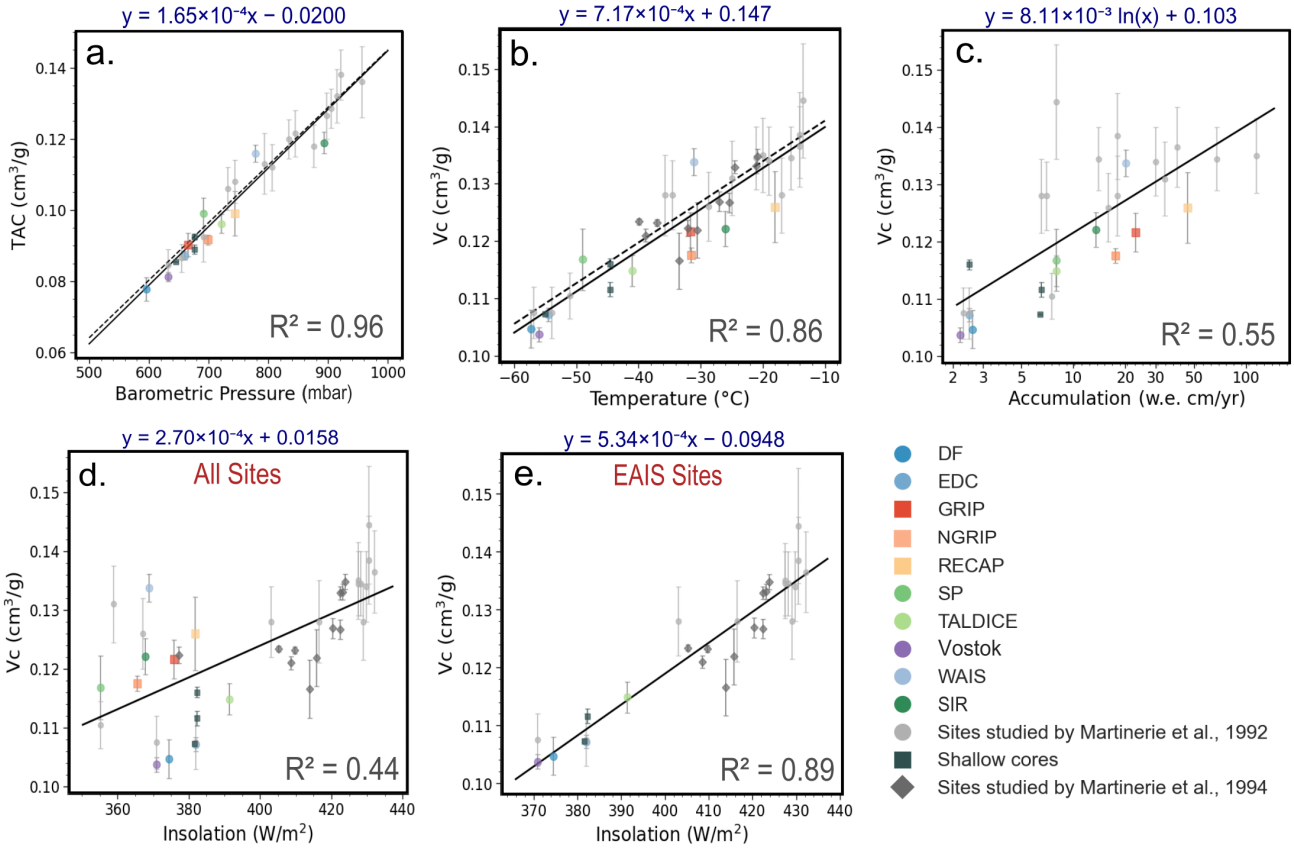

Figure 7. Scatterplots of the relationship between **a.** TAC (V) values (Table 3) and local atmospheric pressure (Table 1), **b.** V_c values (Table 3) and Present-day Temperatures (Table 1), **c.** Present-day accumulation rates at all compiled sites (Table 1), **d.** Computed Half Year Summer Insolation at all compiled sites (Table 1), **e.** Computed Half Year Summer Insolation at East Antarctic Ice Sheet (EAIS) compiled sites (Table 1) and (f) Present-day accumulation rates at Greenland and West Antarctic sites (Table 1). Linear regressions are in black, dashed lines represent linear regression of Martinerie et al. (1992) compiled sites. Error bars represent the estimated maximum error for the Martinerie et al. (1992) sites and the Martinerie et al. (1994) sites (Lipenkov, personal communication). "Shallow cores" include the BE-OI, B35 and B37 shallow ice cores.

420 Next, we propose to investigate non-thermal influences on pore volume by studying the residual term V_{cr}, which can be described for our present-day spatial analysis as the *non-thermal residual pore volume*. We calculated the V_{cr} following the approach of Raynaud et al. (2007) and subsequent studies (Lipenkov et al., 2011; Eicher et al., 2016; Epifanio et al., 2023). We applied equation (2) to calculate the temperature-dependent component of V_c, then computed the non-thermal residual V_{cr} as:

https://doi.org/10.5194/egusphere-2026-953
Preprint. Discussion started: 26 March 2026

$$V_{cr} = \text{TAC} \cdot \frac{T_c}{P_c} \cdot \frac{P_0}{T_0} - V_c(T_s) \quad (2)$$

where T_c and P_c represent the temperature and pressure at bubble close-off depth, T_s the surface temperature and P_0 and T_0 are standard temperature and pressure. $V_c(T_s)$ is the expected pore volume based on surface temperature, calculated using the empirical relationship of Martinerie et al. (1992).

In line with the observations in Fig. 7.e., we do not observe a correlation with HYSI and V_{cr} for the EAIS sites (Fig. A5.b.), suggesting that the spatial correlation between pore volume and insolation is in fact highlighting the influence of surface temperature as a the main driver for V_c. In other words, the insolation signal at these EAIS sites reflect primarily a temperature signature. For the sites located in Greenland and on the WAIS (Fig. A5.a.), we observe a correlation of V_{cr} with HYSI (R^2 = 0.32). These geographical discrepancies highlight a predominant thermal driver for the EAIS sites linked to local insolation signals. The V_c in Greenland and WAIS sites responds to a combination of parameters including surface temperature, suggesting a possible joint influence of insolation and accumulation rates on metamorphism and close-off timing.

These geographical discrepancies point to different firn densification regimes, suggesting that V_c controls operate through different physical pathways depending on local climatic conditions. The correlation of TAC with V_c-temperature and V_c-HYSI at EAIS sites suggest that insolation acts through summer surface temperature and temperature gradients (Raynaud et al., 2024), which govern grain growth rates in the upper firn (Edwards and Epifanio, 2025). By contrast, Greenland and WAIS sites, exposed to lower HYSI than EAIS sites or very high accumulation rates (some similar to EAIS sites), depart from this pattern. While some coastal EAIS sites also experience cloudiness and dynamic weather (Bromwich et al., 2012; Wille et al., 2021), they remain under high HYSI to maintain an insolation control on snow metamorphism. In contrast, Greenland and WAIS sites combine lower HYSI with greater cloudiness, which together reduce the effectiveness of direct insolation on near-surface processes. This supports the idea that, below a HYSI threshold, accumulation-driven processes could dominate. Rapid burial limits the time available for vapour metamorphism and grain rounding, resulting in different firn structures with distinct densification behaviours (Alley et al., 1982; Freitag et al., 2004; Eicher et al., 2016). Variability in layering, stratigraphic effects, and transient firn responses further complicate the V_c signal (Gregory et al., 2014). This dual-threshold regime behaviour could explain why some EAIS sites with both high accumulation and high HYSI still follow the insolation trend, whereas high-accumulation Greenland sites with lower HYSI do not.

The distinct regional patterns become clearer when examining the temperature-accumulation relationships across our compiled sites (Fig. 8.a.). While a general positive correlation exists between temperature and accumulation rates, the relationship exhibits scatter and different regional slopes. EAIS sites show a distinct temperature-accumulation trajectory compared to Greenland and WAIS sites, reflecting different climatic regimes where accumulation is variably coupled to temperature depending on factors such as coastal versus interior positioning, katabatic wind redistribution effects, and regional atmospheric circulation patterns (Nicola et al., 2023). These regional differences are further influenced by variations in storm track activity and cyclonic systems that deliver moisture to different parts of Antarctica (Marshall et al., 2017). The regional heterogeneity in climate-accumulation coupling thus provides additional context for understanding why V_c controls vary between polar regions.

https://doi.org/10.5194/egusphere-2026-953
Preprint. Discussion started: 26 March 2026

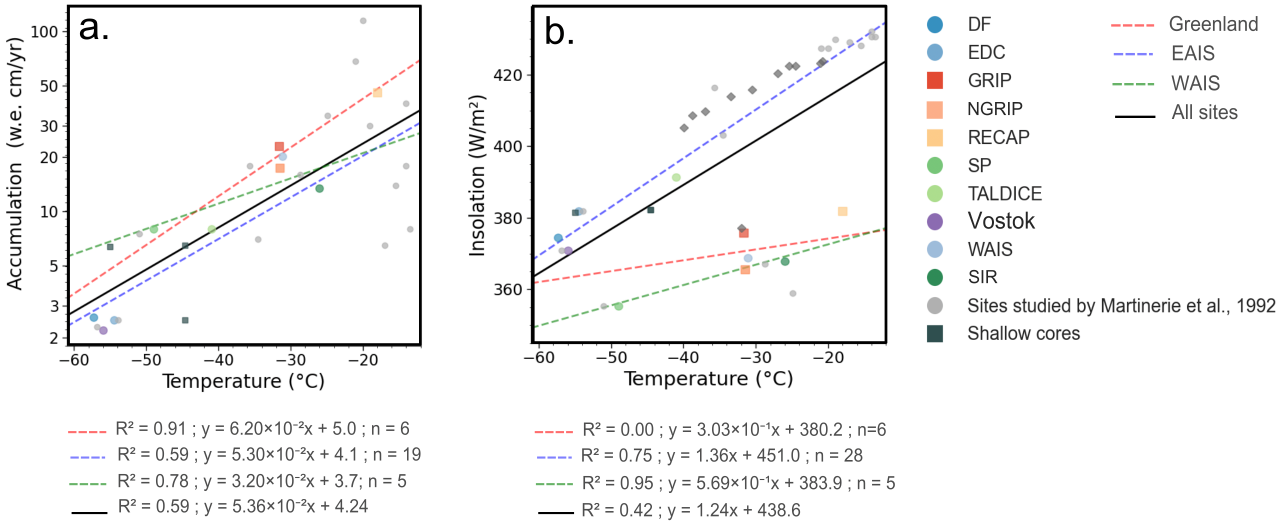

Figure 8. Temperature relationships across polar ice core sites. Scatter plots showing **a.** present-day accumulation rates versus mean annual temperature and **b.** insolation versus mean annual temperature for compiled ice core sites (Table 1). Linear regression lines show distinct regional slopes, highlighting different climatic regimes for EAIS sites (blue), Greenland sites (red) and WAIS sites (green)

The regional differentiation becomes even more pronounced when examining temperature-insolation relationships (Fig. 8.b.). Here, two distinct groups can be identified: EAIS sites form a cluster at higher insolation values, while Greenland and WAIS sites cluster together at lower insolation values.

Together, these findings argue against a unique parametrization of V_c and instead support a regime-dependent interpretation: in high-HYSI environments, grain size–controlled densification dominates and imprints a thermal–orbital signal on V_c (Epifanio et al., 2023), while in low-HYSI, high-accumulation regimes, V_c becomes more sensitive to accumulation dynamics and firn stratigraphy (Eicher et al., 2016). Future efforts should target high-resolution TAC data and micro-structural firn observations to constrain the thresholds and transitions shaping the pore volume signal and better understand temperature gradients in the firn column.

4.2 Relative influence of surface climate parameters at orbital- and millennial scales on the TAC signal

The compiled TAC records across Antarctica and Greenland (Fig. 4., 5., 6., Table 2.) reveal variations at both orbital- and millennial-scales. Across multiple sites, we observe a coherent anti-correlation between TAC and HYSI over time, consistent with earlier interpretations linking TAC to orbital-scale local insolation variation (Raynaud et al., 2007; Lipenkov et al., 2011; Skakun and Lipenkov, 2016; Eicher et al., 2016). We analysed this orbital signal at EDC over 800 ka (Fig. A3.a.) where the obliquity-paced 40 kyr component dominates the TAC CWT-spectrum, while the 100 kyr cycle is less pronounced, as shown previously over the 0-440 ka interval (Raynaud et al., 2007, 2024). Considering that δD is dominated by a 100 kyr-pacing (Fig.

https://doi.org/10.5194/egusphere-2026-953
Preprint. Discussion started: 26 March 2026

A3.c.) and that HYSI signal is not (Fig. A3.b.), we explain the previous spectral analyses by our regression analyses, which show that the combined influence of HYSI and temperature captures long-term TAC variability more effectively than insolation, simulated summer temperature or filtered TAC (Fig. A3.e.) alone. Our results suggest that HYSI governs the baseline evolution of TAC, while millennial-scale climate variations (such as during deglaciations) impose second-order effects through shifts in surface conditions (Table 3.). In particular, during glacial terminations, the amplitude of TAC anomalies increases relative to the insolation baseline, highlighting the additional role of accumulation and temperature in shaping firn properties at orbital scales (Fig. 5.).

Table 3. Summary of V_c control mechanisms across polar regions

Parameter	**Proposed process**	**Temporal-scale**	**HYSI threshold**	**Expression**
Radiative (HYSI)	Summer temperature gradients → grain metamorphism	Orbital	**Higher HYSI**	TAC anti-correlated with HYSI
Thermal + Mechanical (annual temp. + acc. rates)	Rapid burial + compaction limit grain growth and reduce V_c. Overriding of insolation effects	Orbital + Millennial	**Lower HYSI**	TAC decoupled from HYSI: acc./temp. becomes dominant. Peaks during deglaciations.

In addition to the orbital-scale TAC variations, our new EDC high resolution dataset over the time interval 220-430 ka enables to detect millennial-scale TAC changes (Fig. 6.) as already observed at NGRIP and SP (Eicher et al., 2016; Epifanio et al., 2023). These millennial-scale variations occur predominantly during periods of rapid climate change (Fig. 6.). TAC changes vary also in amplitude across sites when examining the last glacial-interglacial transition (Table 4.), with the largest TAC decrease observed at RECAP (-10.9%), followed by DF (-5.8%), NGRIP (-5.8%), and SP (-4.2%). In contrast, EDC shows a minimal response (-0.8%), while WAIS and RICE display opposite trends with TAC increases ($+2.8\%$ and $+4.5\%$, respectively). These contrasting amplitudes are consistent with previous studies showing that millennial-scale TAC responses are site-specific and depend on local accumulation rates and temporal variability. For instance, TAC decreases observed in NGRIP during DO events have been attributed to abrupt increases in accumulation, which reduce pore volume through firn compression (Eicher et al., 2016). Conversely, at SP, during Antarctic Isotope Maxima (AIM) events, accumulation correlates positively with TAC (Epifanio et al., 2023), low accumulation allowing solar temperature gradients to affect grains for a longer time. These contrasting behaviours point to a common mechanism—grain-size modulation—driven by different forcings at different sites.

This site-dependent variability is also evidenced when examining in parallel changes in TAC and in HYSI over the last 25 ka for a selection of Greenland and Antarctic sites (Fig. 9.). While the glacial interglacial HYSI change is of comparable magnitude across sites (1–2%), the amplitude of the TAC changes between the glacial period and the Holocene varies from -11 to +1%. In particular, sites exposed to higher mean summer insolation (above 360-370 (W/m^2)) during the Holocene (e.g.,

https://doi.org/10.5194/egusphere-2026-953
Preprint. Discussion started: 26 March 2026

Table 4. Site-specific comparison of TAC (cm^3/g) and HYSI (W/m^2) values between Holocene and the end of the last glacial period, showing percentage changes (sites ordered by decreasing present-day HYSI)

Site	TAC Holocene	TAC Glacial	ΔTAC	HYSI Holocene	HYSI Glacial	Δ HYSI
RECAP	0.0876	0.0983	-10.9%	395	390	+1.3%
GRIP	0.0867	0.0907	-4.3%	390	385	+1.4%
NGRIP	0.0880	0.0935	-5.8%	379	373	+1.5%
TALDICE	0.0981	0.1013	-3.1%	388	383	+1.3%
EDC	0.0879	0.0886	-0.8%	380	374	+1.4%
DF	0.0814	0.0859	-5.2%	370	368	+0.6%
Vostok	0.0837	0.0877	-4.6%	369	363	+1.6%
WAIS	0.1153	0.1121	+2.8%	367	361	+1.6%
RICE	0.1452	0.1389	+4.5%	367	361	+1.6%
SP	0.0918	0.0958	-4.2%	354	348	+1.8%

RECAP, GRIP, NGRIP, TALDICE) show consistent TAC decreases from glacial to interglacial (Table 5.), roughly following the insolation trajectory (Fig. 9.). In contrast, sites with HYSI lower than about 365 W/m^2 (e.g. WAIS, RICE, and SP) show an increase or minimal change in TAC despite a similar insolation increase (Table 4.).

This inversion of behaviour suggests that TAC responses across the glacial cycle are not solely controlled by HYSI but also depend on the site's position relative to a climatic thresholds (temperature, accumulation) or insolation threshold as suggested in Table 3. This glacial-interglacial transition thus provides a natural experiment demonstrating how sites with different mean insolation values respond to the same orbital forcing. The threshold-like behaviour observed here confirms that TAC cannot be universally interpreted through insolation alone, but requires understanding of the local climatic regime. This potential threshold is further supported by the weak performance of single-variable regressions at SP (Fig. 4.a.), where TAC variations do not align well with insolation trends. This could imply that when insolation falls below a certain level, surface-driven parameters such as burial rate or firn temperature may become the dominant controls on TAC variability, overriding the insolation control that prevails at higher-HYSI sites.

However, these interpretations face site-specific uncertainties: temporal elevation changes affect TAC via P_c and T_c (Equation 1.), and ice flow variations may also influence TAC, though both remain unconstrained here but may also influence TAC responses differently across sites. Insolation control is strongest at cold sites (Vostok, EDC, DF) where winter temperatures below -30°C result in extremely low water vapor concentrations in pores, hindering structural changes and concentrating grain growth to summer months (Raynaud et al., 2007), and weaker at high-accumulation sites where rapid burial shortens surface exposure, though HYSI-TAC correlations remain significant (GRIP, NGRIP) (Fig. 4.). Overall, our findings confirm that TAC integrates multiple levels of climatic control: an orbital-scale control related to local summer insolation, a more irregular control at shorter timescales related to changes in surface conditions, and possibly long-term variations associated with surface eleva-

https://doi.org/10.5194/egusphere-2026-953
Preprint. Discussion started: 26 March 2026

tion changes (Table 3). Importantly, the strength and coherence of these components vary by site, implying that TAC cannot be interpreted without accounting for both the timescale, local surface parameters and the local firn densification processes.

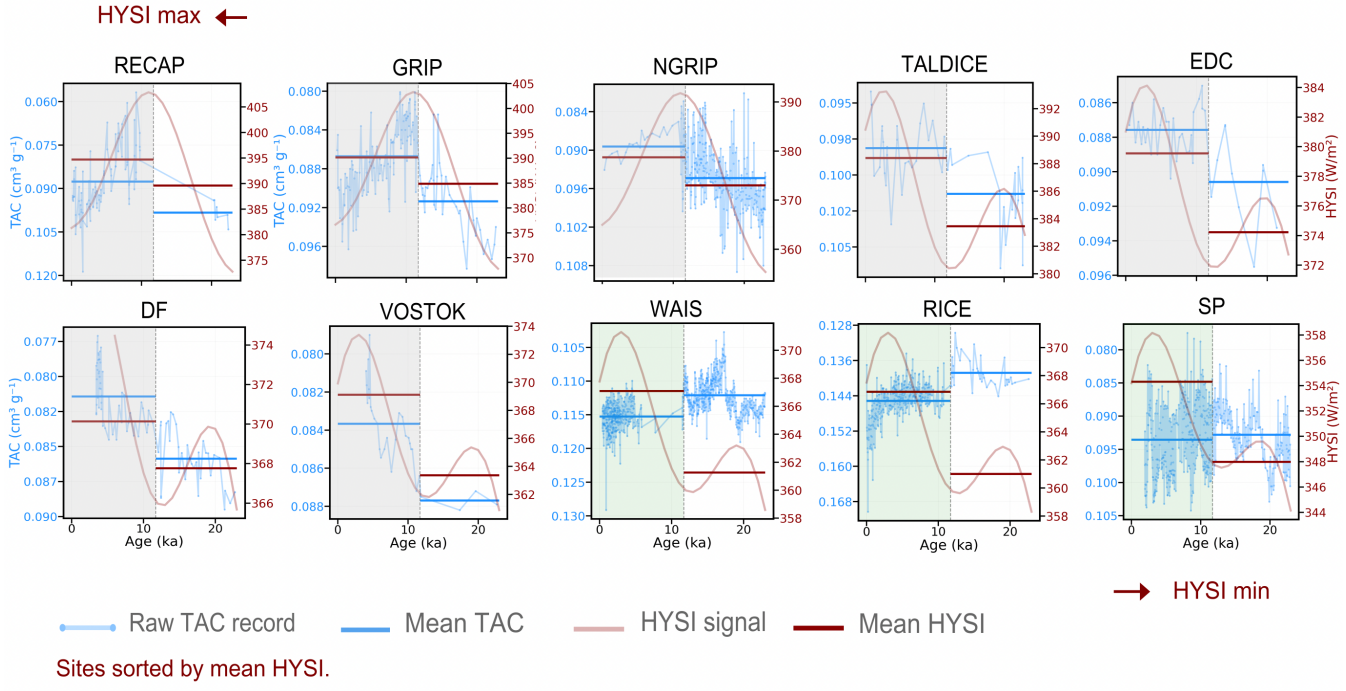

Figure 9. Temporal changes of TAC (in blue) and HYSI (in red) across the last 25 ka, sorted by decreasing HYSI. Grey shading marks the Holocene, green the Holocene period where TAC increases, and white the end of the last glacial period (e.g. between 11.7 and 25 ka). Blue and red horizontal lines denote Holocene and glacial means. TAC is shown on a reversed scale.

4.3 Implications for the use of TAC as an orbital dating tool

While TAC archives preserves orbital-scale variability paced by local summer insolation, our analyses demonstrate that insolation alone does not fully capture TAC amplitude variations. Incorporating surface temperature alongside HYSI better reproduces the measured signal (Fig. 5., 6.), indicating that surface climate modulates the expression of orbital forcing in the firn. This temperature influence is further evidenced by CWT spectral analysis (Fig. A3.), showing that while HYSI lacks significant 100 kyr variability, the raw TAC signal contains pronounced 100 kyr cycles. The deviation between measured TAC and the TAC predicted only from HYSI during terminations illustrates this point: while orbital cyclicity is present in both signals, temperature effects introduce phase shifts and amplitude distortions (Fig. 5., 10.). We computed a temperature-corrected TAC record at EDC by removing the temperature-dependent component from the TAC-signal (Fig. 10.) and as detailed it in A1. for the method. Spectral analysis reveals that this correction eliminates much of the 100 kyr variability present in raw TAC. The resulting spectrum (Fig. A3.d.) closely resembles the HYSI spectral signature (Fig. A3.b.), demonstrating that temperature effects can mask the underlying orbital signal, thus affecting its use in orbital dating.

https://doi.org/10.5194/egusphere-2026-953
Preprint. Discussion started: 26 March 2026

To assess the impact of temperature correction on orbital tuning, we compare raw TAC and temperature-corrected TAC (both on AICC2023 chronology) with the HYSI target to examine whether correction affects the timing and position of TAC maxima and minima. During TII ($\sim$ 135-130 ka) and TIV ($\sim$ 340-335 ka), the corrected signal exhibits enhanced alignment with the HYSI target, suggesting that temperature effects can mask or amplify the underlying insolation signal during periods of millennial-scale climate change (Fig. 10.). Notably, the correction reveals two distinct peaks in corrected-TAC (labelled "New TAC-peak") that are not visible in the uncorrected record, providing additional tie-points for orbital dating(Fig. 10.b.). More tie-points have been identified in the entire record over the past 800 ka but will be shown in a separate study. Moreover, phase differences between measured and temperature-corrected TAC reach up to 2-5 ka during these terminations (Fig. 10.). For ice cores where TAC serves as a primary orbital dating tool, the phase relationships must be considered when establishing tie-points, as purely insolation-based tuning may introduce systematic age offsets of several millennia during critical climate transitions. Recent studies comparing TAC-based orbital chronologies between different Antarctic sites have confirmed similar levels of uncertainty, with coherent timescales showing deviations typically within 2 ka when compared to optimized multi-parameter chronologies (Khomyakova et al., 2025).

The corrections shown here use reconstructed surface temperature (T_s) rather than close-off temperature (T_c), which requires justification given the complex and not fully understood physical mechanisms linking temperature to TAC (Raynaud et al., 2007, 2024; Edwards and Epifanio, 2025; Khomyakova et al., 2025). While T_c controls (along with P_c) the density of air in closed pores through the ideal gas effect, it cannot control pore volume (V_c) itself, which forms over hundreds to thousands of years as snow travels through the firn column. It is the average temperature experienced during this transit that controls V_c. Consequently, an increase in T_s during warming should increase V_c (and TAC), while an increase in T_c would decrease TAC—opposite effects with different timings (Martinerie et al., 1992). In view of these complexities and uncertainties, we choose T_s with a specific timing simply because it empirically improves the prediction of filtered TAC. Fig. 10 illustrates this: corrected TAC leads measured TAC by 3-5 ka during warmings and lags by 2-3 ka during coolings, consistent with T_s effects. Testing with T_c (results not shown) identifies consistent orbital peaks, confirming the robustness of our approach.

Overall, rather than limiting its utility, TAC's sensitivity to both radiative and climatic influences provides complementary information for orbital dating. By incorporating our improved understanding of temperature and accumulation effects, and by combining TAC with complementary proxies such as O_2/N_2 and atmospheric $\delta^{18}O$ of O_2 (Bouchet et al., 2023; Harris Stuart et al., 2024), we can use TAC's multi-parameter response to strengthen ice core chronologies while gaining insights into past firn conditions. Moreover, this temperature correction approach, which reveals additional tie-points, could prove valuable for dating deep ice cores.

https://doi.org/10.5194/egusphere-2026-953
Preprint. Discussion started: 26 March 2026

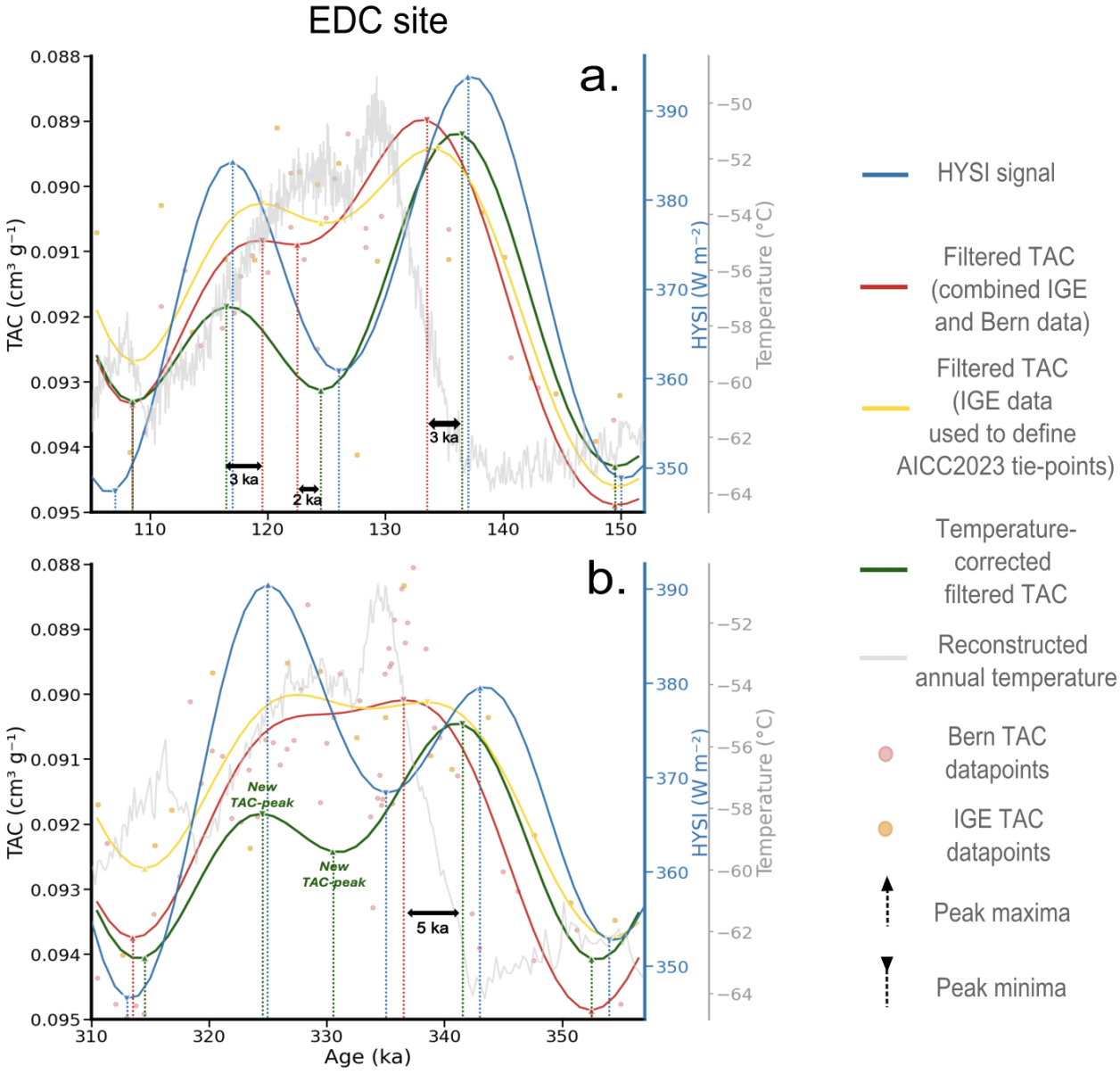

Figure 10. EDC TAC signal and HYSI target over **a.** 105-155 ka time interval covering TII and **b.** 310-360 ka covering TIV. Measured raw TAC from Bern dataset (red dots), measured raw TAC from IGE dataset (yellow dots), filtered composite TAC incorporating Bern + IGE datapoints (red line), filtered TAC signal (IGE datapoints) used for AICC2023 orbital dating exercise (yellow line), temperature-corrected TAC filtered (green line) are shown on the AICC2023 ice age scale (Bouchet et al., 2023). Half Year Summer Insolation (HYSI) target is displayed in blue. All records are filtered using a 16.7 kyr low-pass FIR filter. TAC is shown on a reversed scale. Triangles indicate minima and maxima of each curve. Horizontal grey arrows indicate phase lags (in ka) between tie points based on measured TAC versus temperature-corrected TAC, demonstrating that temperature corrections can shift orbital alignment by 1-5 ka during these transition periods. Annual temperature reconstructions from Jouzel et al. (2007) are used for the temperature corrections (Equation 4, Appendix A1).

https://doi.org/10.5194/egusphere-2026-953
Preprint. Discussion started: 26 March 2026

4.4 Limitations and perspectives

The interpretation of TAC as a proxy for past climate and chronology remains subject to several methodological and physical limitations. In the following, we outline key challenges, and identify promising directions for future research.

- As seen in section 2.5, a primary challenge in interpreting TAC lies in the temporal alignment of the signal (Edwards and Epifanio, 2025). TAC reflects physical processes that occur during pore closure (on the gas-age scale) yet it is measured in the ice matrix, which follows the chronology of ice deposition. This offset (Δage), can exceed several millennia in low-accumulation settings, introducing ambiguity when aligning TAC variations with orbital forcings or other gas-based climate proxies. Given that TAC fundamentally represents air entrapped within the ice matrix, the physical processes controlling TAC theoretically operate on both age scales. This ambiguity manifests differently depending on site conditions: at high-accumulation sites, accumulation variations affect overburden pressure during bubble close-off, causing TAC to correlate with δ^{15}N on the gas age scale (Eicher et al., 2016), while at lower accumulation sites, effects are expressed on the ice age scale because the mechanism controlling TAC is linked to surface grain metamorphism (Epifanio et al., 2023). Our site-by-site comparison of TAC correlations (Table A2, A3) with surface parameters (accumulation and temperature) on both gas and ice timescales reveals that the strength of these relationships can shift depending on the age model employed. In some cases, stronger correlations emerge when TAC is interpreted on the ice-age scale (e.g. Vostok). In contrast, other sites show greater consistency across gas-age scales (e.g. NGRIP). In other cases, the choice of the age scale does not significantly change the result.

- The previously mentioned difference between the surface temperature T_s and the temperature at close-off depth T_c is significant over time and should be taken into account when assessing TAC temporally. However, for the orbital-scale analyses presented here, we verified that using T_s versus T_c does not significantly affect peak identification and main TAC-climate correlations, as both parameters track similar long-term trends. This distinction becomes more critical for sub-orbital or millennial-scale investigations where thermal diffusion and rapid temperature changes under transient climates (Raynaud et al., 2007) may introduce additional complexity. Furthermore, isotope-based temperature reconstructions may carry significant uncertainties, with errors of up to a factor of two at EAIS sites (Buizert et al., 2021), adding an additional limitation for TAC-temperature correlations. For improved temporal analysis of TAC records, future studies (for instance single-site studies) should based their analyses on firn thermal diffusion models (Goujon et al., 2003) to obtain accurate T_c.

- Firn densification models indeed represent a critical area for development for predicting close-off depth and porosity, directly controlling TAC. Firn densification models such as developed by Goujon et al. (2003) parametrize densification through temperature, accumulation-rates, and grain-geometry evolution, without explicitly accounting for insolation-driven metamorphism in the upper firn layers. An improved model would need to incorporate the competing effects of insolation, accumulation, and grain size evolution on porosity and bubble close-off. Our results suggest that threshold behaviour may exist where firn properties transition between insolation and accumulation-dominated regimes (depending on site-specific combinations of HYSI), temperature, and snow burial rate. Identifying and parametrizing such thresholds in firn models would improve mechanistic predictions of TAC variability under different climate conditions.

https://doi.org/10.5194/egusphere-2026-953
Preprint. Discussion started: 26 March 2026

- The sparse availability of high-resolution TAC datasets across sites and periods further limits our ability to fully characterize TAC variability at both orbital- and millennial scales. Still, our new compilation highlights that millennial-scale variability is present in several Greenland and Antarctic TAC records. Expanding high-resolution TAC measurements in polar ice core from both hemispheres, especially at various accumulation and insolation sites, is necessary to refine spatial patterns and identify systematic responses to orbital- and millennial-scale forcing.

- Originally, the sensitivity of TAC to surface atmospheric pressure offers a pathway for reconstructing past surface elevations Raynaud and Lebel (1979). However, our results confirm that the TAC signal is strongly modulated by the pore volume at close-off (Martinerie et al., 1992; Raynaud et al., 2007), which itself depends on firn microstructure, temperature gradients, and accumulation. In this context, elevation-induced pressure changes may be indistinguishable from firn-structure-driven variations. Nevertheless, if V_c can be reliably reconstructed, either through empirical regression or physical modelling, the pressure (and thus elevation) signal embedded in TAC may be recoverable. In particular, our spatial-scale analysis shows that sites with similar elevations but different summer insolation display distinct TAC levels, pointing to the importance of accurately capturing insolation-driven firn processes when using TAC to infer elevation.

- In addition, understanding how surface metamorphism translates to pore volume at close-off and thus TAC requires better quantification of secondary factors. For example, dust content has been shown to modify grain boundary migration (Hörhold et al., 2012), potentially impacting firn permeability and close-off porosity. Similarly, wind-driven compaction can introduce significant heterogeneity in the upper firn column (Martinerie et al., 1994), altering the efficiency of air trapping. Studies combining firn density and microstructure measurements (Freitag et al., 2004; Hörhold et al., 2011) across climatically diverse sites could help refine knowledge gaps on firn dynamics impacting TAC.

5 Conclusions

This study presents new TAC measurements from EDC, TALDICE, EDML, and shallow ice cores BEOI, B34 and B37. Multiple regression analyses show that HYSI combined with annual temperature or accumulation rates best explains TAC changes, capturing both orbital- and millennial-scale signals. This multi-scale behaviour is particularly pronounced during deglaciations, when rapid surface climate changes modulate the insolation-driven background. Spatial-scale analysis across compiled sites extends the linear relationships of TAC and V_c with surface parameters (atmospheric pressure, temperature, accumulation and insolation) to a broader range of polar locations. We examine for the first time the relationship between V_c and insolation, revealing strong regional contrasts. EAIS sites exhibiting strong correlations between V_c and HYSI ($R^2 = 0.89$), while Greenland and WAIS sites show weaker correlations. Our results suggest that the dominant controls on V_c vary across sites. At cold, high-insolation sites (high EAIS plateau and some coastal EAIS), summer insolation drives V_c through surface grain metamorphism. At sites with lower HYSI or warmer conditions, multiple climate parameters contribute to V_c variability. Further high-resolution records (notably at high HYSI coastal sites) are needed to fully resolve these controls across different climatic settings.

https://doi.org/10.5194/egusphere-2026-953
Preprint. Discussion started: 26 March 2026

Given that surface temperature and accumulation modulate TAC alongside insolation during terminations, applying temperature corrections before TAC-HYSI alignment can improve orbital tie point accuracy. Although TAC remains a valuable orbital dating tool to constrain the ice core chronologies, temperature-corrected TAC signals can show phase differences of 1-5 ka with the raw TAC signal during terminations, emphasizing the importance of using TAC in combination with other orbital proxies such as O_2/N_2 rather than as a stand-alone orbital dating tool.

In summary, TAC represents a promising yet complex proxy integrating surface climate, firn physics, and orbital forcing. While its application as an orbital dating tool remains of prime interest, our results demonstrate that improved understanding of V_c controls is essential both for refining TAC-based chronologies and for advancing its potential applications in paleoclimate reconstruction, including past ice sheet elevation estimates. Unlocking this potential will require targeted data, refined models, and a deeper understanding of the processes controlling air trapping in polar firn.

https://doi.org/10.5194/egusphere-2026-953
Preprint. Discussion started: 26 March 2026

6 Appendix

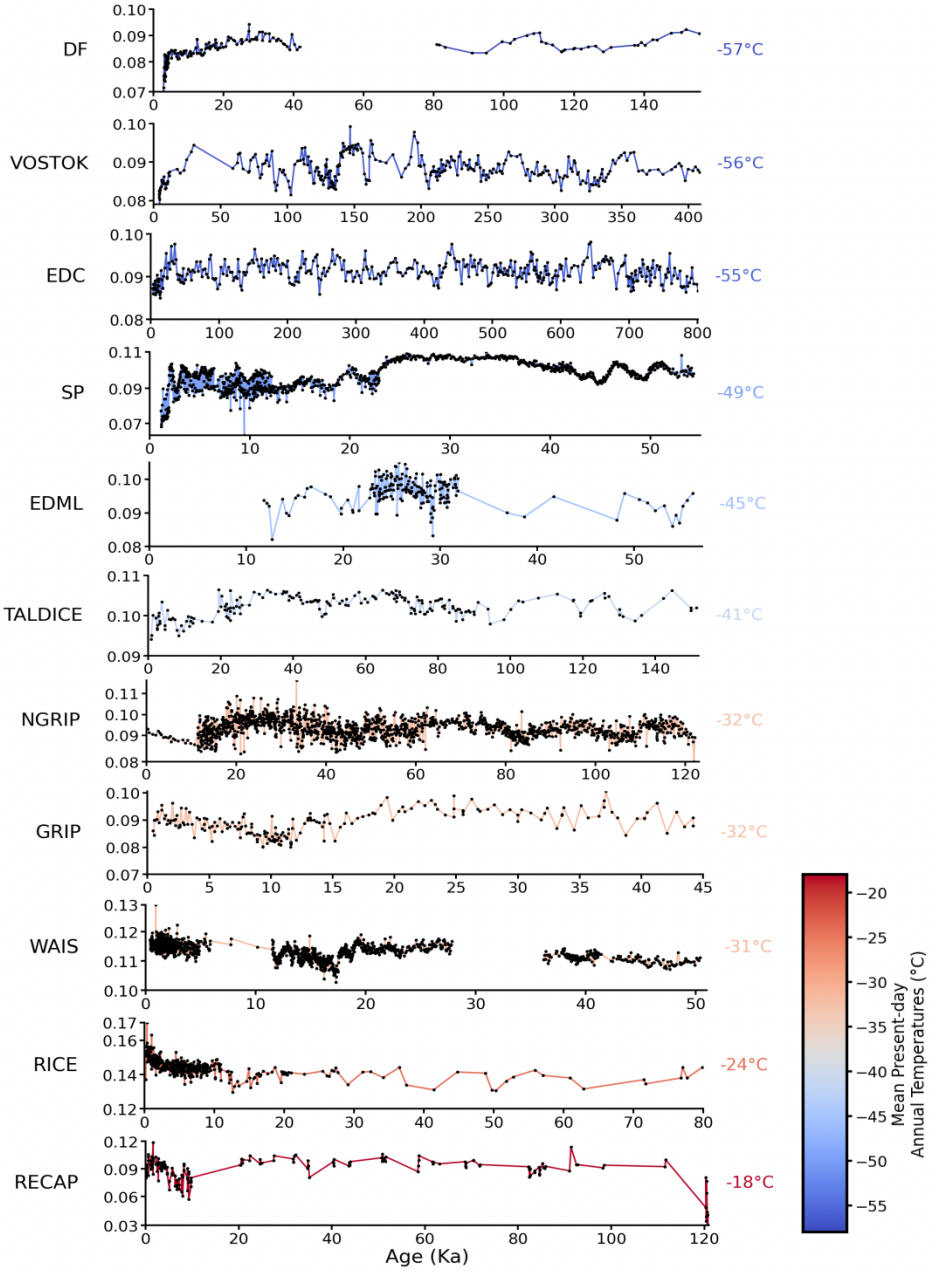

Figure A1. Raw TAC datasets covering at least 40 ka (Table 2.). Sites are sorted from the coldest (DF) to the warmest (RECAP) annual present-day temperature (Table 1.)

https://doi.org/10.5194/egusphere-2026-953
Preprint. Discussion started: 26 March 2026

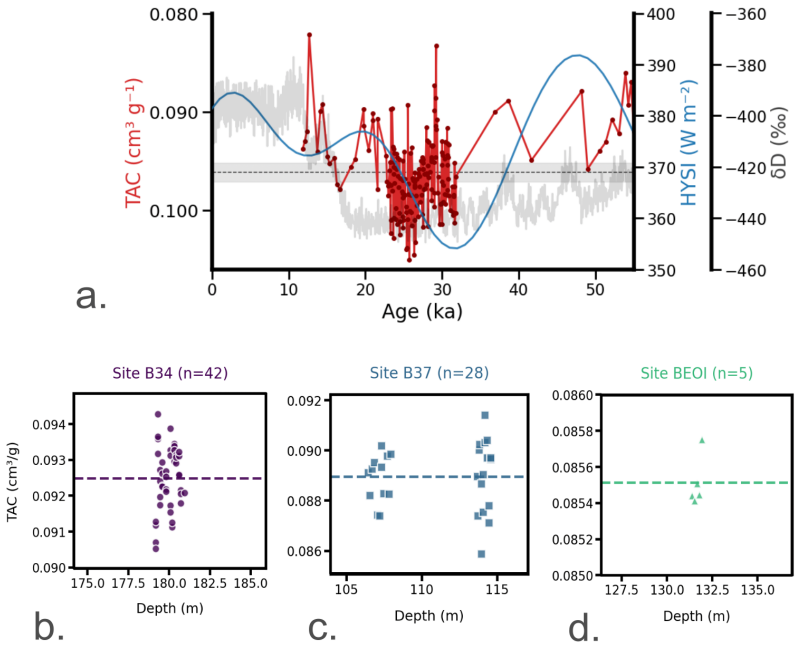

Figure A2. The EDML and new shallow cores TAC records. **a.** EDML record displayed on the AICC2023 ice age scale (Bouchet et al., 2023) and superimposed with the corresponding Half Year Summer Insolation (HYSI) index (in blue) and the EDC δD record (in grey, Jouzel et al. (2007)). TAC is shown on a reversed scale. The dashed black line represents the mean V value over TAC dataset associated with the typical 1.5% analytical uncertainty range in grey. The Shallow cores **b.** B34; **c.** B37 and **d.** BEOI displayed against depth with their mean value (dashed horizontal line)

https://doi.org/10.5194/egusphere-2026-953
Preprint. Discussion started: 26 March 2026

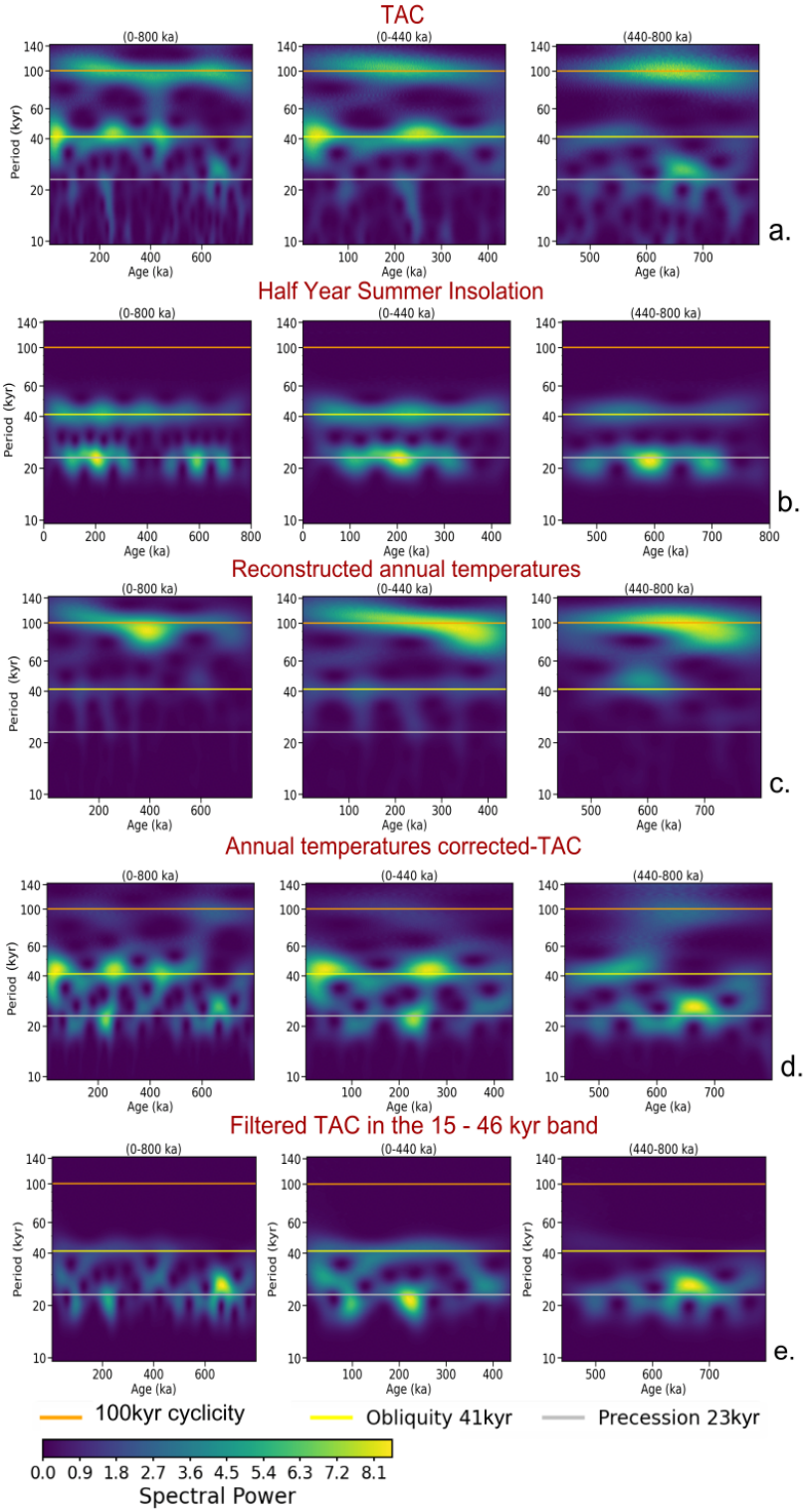

Figure A3. Continuous Wavelet Transform (CWT) Analysis at EDC over the past 800 ka for **a.** TAC **b.** Half Year Summer Insolation (HYSI) **c.** Reconstructed annual temperature (Jouzel et al., 2007), **d.** TAC temperature-corrected records and **e.** TAC time series filtered in the 15–46 kyr band often used in orbital dating. Records are shown on the AICC2023 ice age scale (Bouchet et al., 2023).

https://doi.org/10.5194/egusphere-2026-953
Preprint. Discussion started: 26 March 2026

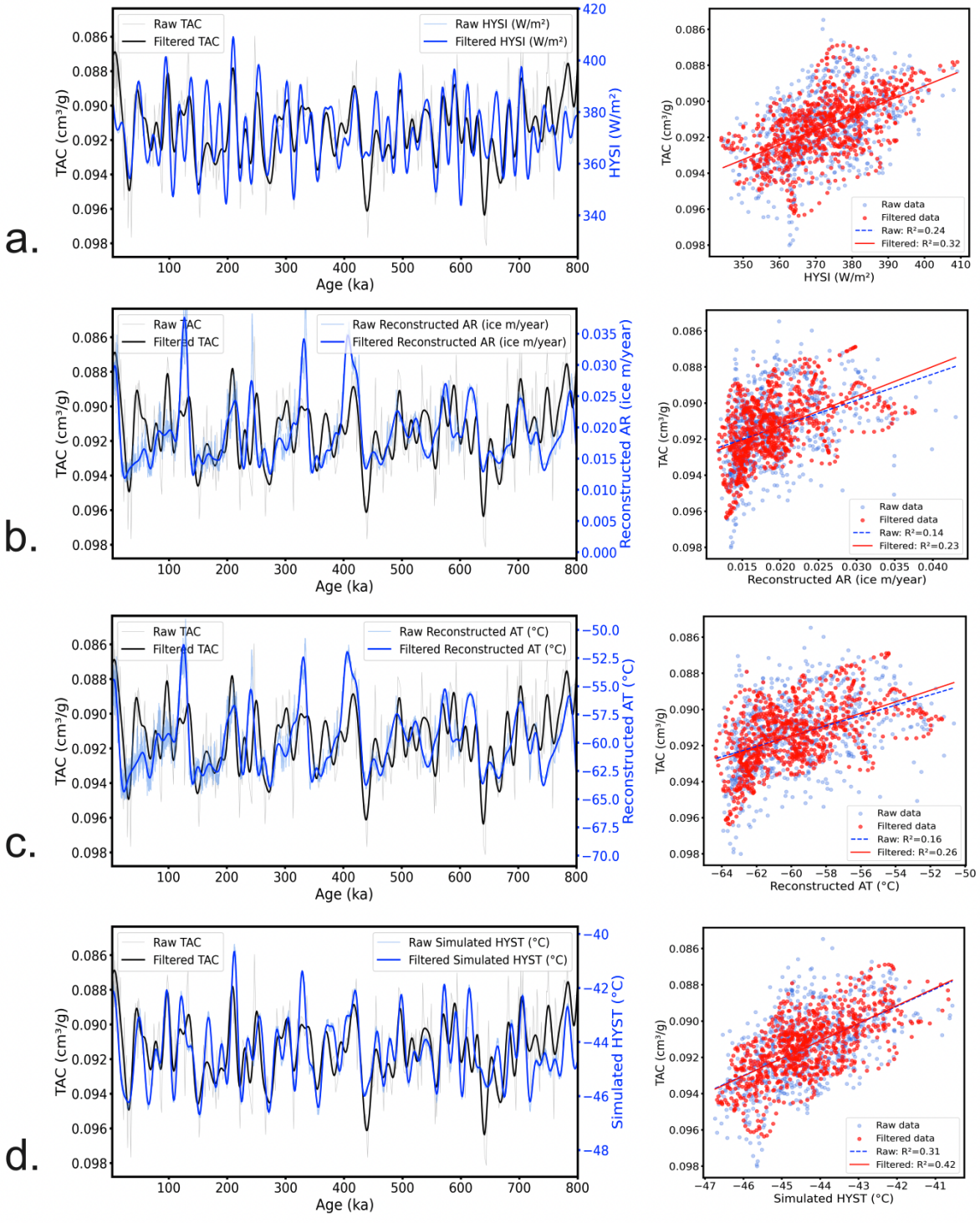

Figure A4. Simple linear regressions of TAC at EDC with a. Half Year Summer Insolation (HYSI), b. Reconstructed Annual Accumulation Rates (AR) c. Reconstructed Annual surface Temperature(AT) d. Simulated Half Year Temperatures (HYST). References are available in Table 2.

https://doi.org/10.5194/egusphere-2026-953
Preprint. Discussion started: 26 March 2026

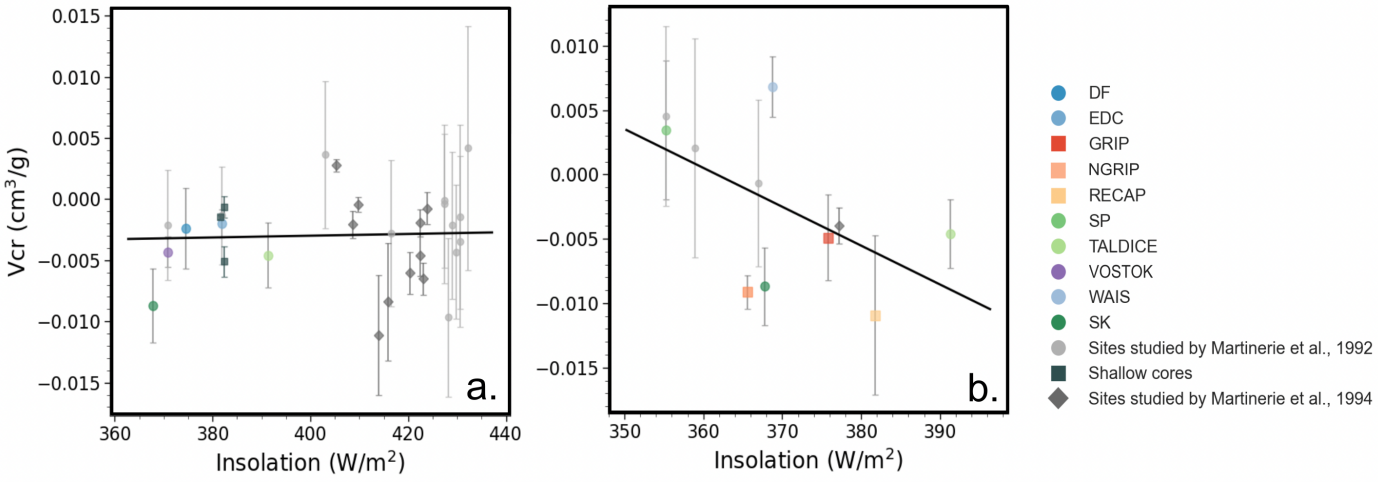

Figure A5. Scatterplots of the relationship between TAC (Vcr) values, e.g. non-thermal residual of pore volume (Table 3) and Computed Half Year Summer Insolation at all compiled sites (Table 1); for **a.** EAIS sites ($R^2 = 0.0$) and **b.** WAIS and Greenland sites ($R^2 = 0.32$). Linear regressions are in black. Error bars represent the estimated maximum error for the Martinerie et al. (1992) sites and the Martinerie et al. (1994) sites (Lipenkov, personal communication). For the other compiled sites, the error bars correspond to the standard deviation. "Shallow cores" include BE-OI, B35 and B37 data at shallow depths

Table A1: Total air content (TAC), calculated pore volume (V_c), and non-thermal residual (V_{cr}) for compiled ice cores over the past millenia. V and V_{cr} of the Martinerie et al. (1994) sites will be published in a future study.

Core	TAC (cm^3/g)	V_c (cm^3/g)	V_{cr} (cm^3/g)	Method	Datapoints	Depth interval (m)
Ice cores compiled in this study						
DF	0.0778	0.1047	-0.0023	Oyabu et al. (2020)	19	120.68-135.20
EDC	0.0872	0.1072	-0.0020	Lipenkov et al. (1995)	3	115-138
GRIP	0.0903	0.1216	-0.0049	Lipenkov et al. (1995)	10	122-320
NGRIP	0.0916	0.1194	-0.0091	Schmitt et al. (2014); Eicher et al. (2016)	3	133-326
RECAP	0.0990	0.1260	-0.0109	Lipenkov et al. (1995); Fegyveresi (2015)	-	see Vudayagiri et al. (2025)
RICE	0.1522	0.1551	0.0224	Mitchell et al. (2015)	35	70-210
SP	0.0970	0.1192	0.0034	Mischler et al. (2009); Fegyveresi (2015)	22	193-234
TALDICE	0.0961	0.1148	-0.0046	Schmitt et al. (2014)	4	91-133
Vostok	0.0814	0.1037	-0.0043	Lipenkov et al. (1995)	35	70-210
WAIS	0.1159	0.1338	0.0068	Schmitt et al. (2014)	60	121-264
SIR	0.1189	0.1221	-0.0087	Wolff et al. (2024)	41	70-144

Continued on next page

https://doi.org/10.5194/egusphere-2026-953
Preprint. Discussion started: 26 March 2026

Table A1 – continued from previous page

Core	TAC (cm^3/g)	V_c (cm^3/g)	V_{cr} (cm^3/g)	Method	Datapoints	Depth interval (m)
Martinerie et al. (1992) cores - see Martinerie et al. (1992) for all methods and calculations						
BHJ	0.1360	0.1445	0.0042	–	–	–
BHF	0.1380	0.1365	-0.0035	–	–	–
BHP	0.1320	0.1385	-0.0015	–	–	–
D-10	0.1285	0.1345	-0.0043	–	–	–
BHB	0.1265	0.1280	-0.0097	–	–	–
BHQ	0.1180	0.1340	-0.0022	–	–	–
DE08	0.1215	0.1350	-0.0004	–	–	–
BHD	0.1200	0.1345	-0.0001	–	–	–
Byrd	0.1120	0.1310	-0.0007	–	–	–
Camp Century	0.1130	0.1310	0.0021	–	–	–
D-57	0.1080	0.1260	-0.0028	–	–	–
Mizuho	0.1060	0.1280	0.0036	–	–	–
South Pole	0.0925	0.1280	0.0045	–	–	–
Dome C	0.0865	0.1105	-0.0013	–	–	–
Vostok	0.0845	0.1075	-0.0021	–	–	–
Martinerie et al. (1994) cores - see Martinerie et al. (1994) for all methods and calculations						
KM-60	unpublished	0.1340	-0.0007	–	–	–
KM-73	unpublished	0.1280	-0.0065	–	–	–
KM-105	unpublished	0.1300	-0.0019	–	–	–
KM-140	unpublished	0.1240	-0.0060	–	–	–
KM-200	unpublished	0.1190	-0.0084	–	–	–
KM-260	unpublished	0.1140	-0.0110	–	–	–
KM-325	unpublished	0.1220	-0.0004	–	–	–
KM-369	unpublished	0.1190	-0.0021	–	–	–
KM-400	unpublished	0.1230	0.0028	–	–	–
D-47	unpublished	0.1267	-0.0046	–	–	–
EUROCORE	unpublished	0.1223	-0.0040	–	–	–
Shallow ice cores (this study)						
B34	0.0925	0.1160	-0.0006	Schmitt et al. (2014)	42	179-181
B37	0.0889	0.1116	-0.0051	Schmitt et al. (2014)	28	106-115
BEOI	0.0855	0.1073	-0.0015	Schmitt et al. (2014)	5	131-132

https://doi.org/10.5194/egusphere-2026-953
Preprint. Discussion started: 26 March 2026

Table A2: Linear regressions plotted on the ice age between TAC in cm^3/g and half year summer insolation (HYSI) in W/m^2, annual accumulation rates (acc) in w.e. cm/yr, annual temperatures (temp), and simulated half year summer temperature (tempsimu) both in °C. DF_1 corresponds to DF between 0-38 ka and DF_2 to DF between 77-151 ka

Site	Parameter	Regression	Equation	R	R^2
DF_1	HYSI	Raw	$y = -3 \times 10^{-4}x + 0.1784$	−0.81	0.65
		Filtered	$y = -4 \times 10^{-4}x + 0.2195$	−0.88	0.78
	acc	Raw	$y = -0.4313x + 0.0954$	−0.81	0.65
		Filtered	$y = -0.6319x + 0.0990$	−0.90	0.81
	temp	Raw	$y = -8 \times 10^{-4}x + 0.0398$	−0.81	0.65
		Filtered	$y = -1.1 \times 10^{-3}x + 0.0197$	−0.92	0.84
DF_2	HYSI	Raw	$y = -1 \times 10^{-4}x + 0.1170$	−0.64	0.42
		Filtered	$y = -1 \times 10^{-4}x + 0.1228$	−0.67	0.45
	acc	Raw	$y = -0.0822x + 0.0881$	−0.22	0.05
		Filtered	$y = -0.1450x + 0.0896$	−0.37	0.13
	temp	Raw	$y = -1 \times 10^{-4}x + 0.0785$	−0.19	0.03
		Filtered	$y = -2 \times 10^{-4}x + 0.0720$	−0.32	0.10
EDC	HYSI	Raw	$y = -1 \times 10^{-4}x + 0.1220$	−0.49	0.24
		Filtered	$y = -1 \times 10^{-4}x + 0.1219$	−0.57	0.32
	acc	Raw	$y = -0.1441x + 0.0942$	−0.37	0.14
		Filtered	$y = -0.1644x + 0.0946$	−0.47	0.22
	temp	Raw	$y = -3 \times 10^{-4}x + 0.0745$	−0.40	0.16
		Filtered	$y = -3 \times 10^{-4}x + 0.0726$	−0.50	0.25
	tempsimu	Raw	$y = -1.0 \times 10^{-3}x + 0.0491$	−0.55	0.30
		Filtered	$y = -1.0 \times 10^{-3}x + 0.0484$	−0.65	0.42
GRIP	HYSI	Raw	$y = -3 \times 10^{-4}x + 0.1893$	−0.82	0.67
		Filtered	$y = -3 \times 10^{-4}x + 0.1921$	−0.91	0.83
	acc	Raw	$y = -0.0342x + 0.0957$	−0.56	0.32
		Filtered	$y = -0.0371x + 0.0960$	−0.75	0.57
	tempsimu	Raw	$y = -5 \times 10^{-4}x + 0.0797$	−0.73	0.53
		Filtered	$y = -5 \times 10^{-4}x + 0.0803$	−0.86	0.74
NGRIP	HYSI	Raw	$y = -1 \times 10^{-4}x + 0.1424$	−0.62	0.39
		Filtered	$y = -1 \times 10^{-4}x + 0.1398$	−0.66	0.43

Continued on next page

https://doi.org/10.5194/egusphere-2026-953
Preprint. Discussion started: 26 March 2026

Table A2 – continued from previous page

Site	Parameter	Regression	Equation	R	R^2
	acc	Raw	$y = -0.0372x + 0.0966$	−0.49	0.24
		Filtered	$y = -0.0445x + 0.0972$	−0.64	0.41
	temp	Raw	$y = -3 \times 10^{-4}x + 0.0828$	−0.45	0.20
		Filtered	$y = -4 \times 10^{-4}x + 0.0771$	−0.71	0.50
	tempsimu	Raw	$y = -7 \times 10^{-4}x + 0.0786$	−0.72	0.52
		Filtered	$y = -7 \times 10^{-4}x + 0.0780$	−0.87	0.75
RECAP	tempsimu	Raw	$y = -1.2 \times 10^{-3}x + 0.0899$	−0.37	0.14
		Filtered	$y = -1.5 \times 10^{-3}x + 0.0894$	−0.48	0.23
SP	HYSI	Raw	$y = -3 \times 10^{-4}x + 0.2109$	−0.57	0.32
		Filtered	$y = -4 \times 10^{-4}x + 0.2336$	−0.60	0.36
	acc	Raw	$y = -0.2545x + 0.1120$	−0.62	0.38
		Filtered	$y = -0.3812x + 0.1182$	−0.86	0.74
	temp	Raw	$y = 1.8 \times 10^{-3}x + 0.0044$	0.60	0.36
		Filtered	$y = 2.5 \times 10^{-3}x - 0.0368$	0.76	0.58
	tempsimu	Raw	$y = -2.7 \times 10^{-3}x - 0.0118$	−0.67	0.45
		Filtered	$y = -3.4 \times 10^{-3}x - 0.0403$	−0.77	0.59
TALDICE	HYSI	Raw	$y = -1 \times 10^{-4}x + 0.1352$	−0.47	0.22
		Filtered	$y = -1 \times 10^{-4}x + 0.1368$	−0.52	0.27
	acc	Raw	$y = -0.0688x + 0.1065$	−0.39	0.16
		Filtered	$y = -0.0726x + 0.1067$	−0.44	0.20
Vostok	HYSI	Raw	$y = -1 \times 10^{-4}x + 0.1215$	−0.45	0.20
		Filtered	$y = -1 \times 10^{-4}x + 0.1213$	−0.51	0.26
	acc	Raw	$y = -0.2629x + 0.0934$	−0.44	0.20
		Filtered	$y = -0.3196x + 0.0944$	−0.58	0.34
	temp	Raw	$y = -6 \times 10^{-4}x + 0.0542$	−0.51	0.26
		Filtered	$y = -6 \times 10^{-4}x + 0.0506$	−0.62	0.38
	tempsimu	Raw	$y = -1.4 \times 10^{-3}x + 0.0239$	−0.57	0.32
		Filtered	$y = -1.4 \times 10^{-3}x + 0.0240$	−0.64	0.41

https://doi.org/10.5194/egusphere-2026-953
Preprint. Discussion started: 26 March 2026

Table A3. Linear regressions plotted on the gas age between TAC in cm^3/g and annual accumulation rates (acc) in w.e. cm/yr and annual temperatures (temp) in °C. DF_1 corresponds to DF between 0-38 ka and DF_2 to DF between 77-151 ka

Site	Parameter	Regression	Equation	R	R^2
DF_1	acc	Raw	$y = -4.408 \times 10^{-1}x + 0.0956$	−0.80	0.64
		Filtered	$y = -6.662 \times 10^{-1}x + 0.0998$	−0.90	0.80
	temp	Raw	$y = -8 \times 10^{-4}x + 0.0384$	−0.80	0.65
		Filtered	$y = -1.2 \times 10^{-3}x + 0.0446$	−0.90	0.80
DF_2	acc	Raw	$y = -2.031 \times 10^{-1}x + 0.0915$	−0.43	0.18
		Filtered	$y = -2.719 \times 10^{-1}x + 0.0930$	−0.56	0.31
	temp	Raw	$y = -8 \times 10^{-4}x + 0.0384$	−0.80	0.65
		Filtered	$y = -1.1 \times 10^{-3}x + 0.0157$	−0.91	0.84
EDC	acc	Raw	$y = -1.364 \times 10^{-1}x + 0.0941$	−0.36	0.13
		Filtered	$y = -1.542 \times 10^{-1}x + 0.0944$	−0.45	0.21
	temp	Raw	$y = -3 \times 10^{-4}x + 0.0753$	−0.39	0.15
		Filtered	$y = -3 \times 10^{-4}x + 0.0736$	−0.48	0.24
GRIP	acc	Raw	$y = -4.24 \times 10^{-2}x + 0.0975$	−0.67	0.45
		Filtered	$y = -4.42 \times 10^{-2}x + 0.0979$	−0.83	0.70
	temp	Raw	$y = 9 \times 10^{-4}x + 0.1189$	0.49	0.24
		Filtered	$y = 8 \times 10^{-4}x + 0.1158$	−0.62	0.38
NGRIP	acc	Raw	$y = -4.44 \times 10^{-2}x + 0.0976$	−0.65	0.42
		Filtered	$y = -4.87 \times 10^{-2}x + 0.0980$	−0.76	0.58
	temp	Raw	$y = -3 \times 10^{-4}x + 0.0795$	−0.64	0.41
		Filtered	$y = -4 \times 10^{-4}x + 0.0760$	−0.82	0.68
SP	acc	Raw	$y = -2.623 \times 10^{-1}x + 0.1129$	−0.64	0.40
		Filtered	$y = -3.926 \times 10^{-1}x + 0.1191$	−0.87	0.75
	temp	Raw	$y = 1.7 \times 10^{-3}x + 0.0062$	0.60	0.36
		Filtered	$y = 2.5 \times 10^{-3}x - 0.0332$	0.75	0.56
TALDICE	acc	Raw	$y = -6.89 \times 10^{-2}x + 0.1065$	−0.39	0.16
		Filtered	$y = -7.28 \times 10^{-2}x + 0.1068$	−0.45	0.20
Vostok	acc	Raw	-	0.04	0.00
		Filtered	-	0.09	0.00
	temp	Raw	-	0.01	0.00
		Filtered	-	0.03	0.00

A.1 TAC temperature correction for the EDC core (Fig. 10)

To isolate the orbital signal from temperature effects, the TAC is corrected using the regression model from Table A4 (EDC, HYSI + T). The temperature-corrected TAC is calculated as:

https://doi.org/10.5194/egusphere-2026-953
Preprint. Discussion started: 26 March 2026

Table A4. Multiple linear regression results for TAC predictions in Fig. 5

Core	Model	Const.	Coef. HYSI	Coef. Temp	Adj. R^2	RMSE	p-value
Vostok	HYSI + T	0.0830	-8.81×10^{-5}	-6.05×10^{-4}	0.629	0.00144	$< 10^{-85}$
Vostok	HYSI	0.1215	-9.04×10^{-5}	—	0.262	0.00175	$< 10^{-28}$
EDC	HYSI + T	0.1025	-7.72×10^{-5}	-2.95×10^{-4}	0.546	0.00117	$< 10^{-137}$
EDC	HYSI	0.1219	-8.18×10^{-5}	—	0.323	0.00138	$< 10^{-69}$

Note: Units are TAC (cm^3/g), HYSI (W/m^2), Temperature (°C), RMSE (cm^3/g). Data filtered with 16.7 kyr FIR low-pass filter.

Model equation: $\text{TAC} = \beta_0 + \beta_{\text{HYSI}} \times \text{HYSI} + \beta_{\text{temp}} \times T$

where β_0 is Const., β_{HYSI} is Coef. HYSI, and β_{temp} is Coef. Temp.

$$\text{TAC}_{\text{corrected}} = \text{TAC}_{\text{measured}} - \beta_{\text{temp}} \times (T - \overline{T}) \quad (3)$$

where T is the reconstructed annual atmospheric temperature from Jouzel et al. (2007) at a given age, $\overline{T} = -59.86$ °C is the mean temperature over the entire 0-800 ka period, and $\beta_{\text{temp}} = -2.95 \times 10^{-4}$ is the temperature slope from Table A4. By subtracting $\beta_{\text{temp}} \times (T - \overline{T})$, we remove the temperature anomaly effect at each point: when temperature is above average, the measured TAC is increased to compensate for the negative temperature influence, and vice versa. This correction removes temperature-driven variability, isolating the orbital signal and other non-thermal factors that control TAC variations. All datasets are plotted on the AICC2023 ice age (Bouchet et al., 2023).

Author contributions.

HG wrote the manuscript with the contribution of all co-authors. EC, FP, AL and AMK contributed to the conceptualization of the study and the methodology. VL, EC and DR measured the unpublished EDC TAC dataset at IGE. JS, BS and HF measured and shared the unpublished EDC, TALDICE, EDML, B34, B37 and BEOI TAC datasets at Bern University. ZW and QY acquired and shared the Simulated Half Year Summer Temperature through the LOVECLIM 1.3 model. PM, EC, FP, JS and AL contributed to the collection, analysis and interpretation of TAC and V_c records.

Competing interests.

The authors declare that they have no conflict of interest.

Acknowledgements. The research leading to these results has received funding from the French National Research Agency through the *Towards Beyond EPICA (ToBE)* project (ANR-22-CE01-0024) and through the Make Our Planet Great Again HOTCLIM project (ANR-19-

https://doi.org/10.5194/egusphere-2026-953
Preprint. Discussion started: 26 March 2026

MPGA-0001). This work is a contribution to the European Project for Ice coring in Antarctica (EPICA). This is EPICA publication N°XX. We would like to warmly thank Jon S. Edwards, Jenna A. Epifanio and Johannes Freitag for insightful discussions. Finally, we acknowledge the use of DeepL and Claude for assistance in rephrasing and proofreading some sentences in the manuscript.

https://doi.org/10.5194/egusphere-2026-953
Preprint. Discussion started: 26 March 2026

References

R. B. Alley, J. F. Bolzan, and I. M. Whillans. Polar Firn Densification and Grain Growth. *Annals of Glaciology*, 3:7–11, 1982. ISSN 0260-3055, 1727-5644. https://doi.org/10.3189/S0260305500002433. URL https://www.cambridge.org/core/product/identifier/S0260305500002433/type/journal_article.

L. Arnaud. *Modélisation de la transformation de la neige en glace à la surface des calottes polaires: étude du transport des gaz dans ces milieux poreux*. PhD thesis, Université Joseph Fourier - Grenoble 1, Grenoble, 1997.

L. Arnaud, J. M. Barnola, and P. Duval. Physical modeling of the densification of snow/firn and ice in the upper part of polar ice sheets. 2000.

B. Bereiter, S. Eggleston, J. Schmitt, C. Nehrbass-Ahles, T. F. Stocker, H. Fischer, S. Kipfstuhl, and J. Chappellaz. Revision of the EPICA Dome C CO_2 record from 800 to 600 kyr before present. *Geophysical Research Letters*, 42(2):542–549, Jan. 2015. ISSN 0094-8276, 1944-8007. https://doi.org/10.1002/2014GL061957. URL https://agupubs.onlinelibrary.wiley.com/doi/10.1002/2014GL061957.

A. Berger. Long-Term Variations of Daily Insolation and Quaternary Climatic Changes. *Journal of the Atmospheric Sciences*, 35(12): 2362–2367, Dec. 1978. ISSN 0022-4928, 1520-0469. https://doi.org/10.1175/1520-0469(1978)035<2362:LTVODI>2.0.CO;2. URL http://journals.ametsoc.org/doi/10.1175/1520-0469(1978)035<2362:LTVODI>2.0.CO;2.

A. Berger, M. Loutre, and C. Tricot. Insolation and Earth's orbital periods. *Journal of Geophysical Research: Atmospheres*, 98(D6):10341–10362, June 1993. ISSN 0148-0227. https://doi.org/10.1029/93JD00222. URL https://agupubs.onlinelibrary.wiley.com/doi/10.1029/93JD00222.

A. Berger, M.-F. Loutre, and Q. Yin. Total irradiation during any time interval of the year using elliptic integrals. *Quaternary Science Reviews*, 29(17-18):1968–1982, Aug. 2010. ISSN 02773791. https://doi.org/10.1016/j.quascirev.2010.05.007. URL https://linkinghub.elsevier.com/retrieve/pii/S0277379110001435.

A. Berger, Q. Yin, and Z. Wu. Length of astronomical seasons, total and average insolation over seasons. *Quaternary Science Reviews*, 334: 108620, June 2024. ISSN 02773791. https://doi.org/10.1016/j.quascirev.2024.108620. URL https://linkinghub.elsevier.com/retrieve/pii/S0277379124001215.

N. A. N. Bertler, H. Conway, D. Dahl-Jensen, D. B. Emanuelsson, M. Winstrup, P. T. Vallelonga, J. E. Lee, E. J. Brook, J. P. Severinghaus, T. J. Fudge, E. D. Keller, W. T. Baisden, R. C. A. Hindmarsh, P. D. Neff, T. Blunier, R. Edwards, P. A. Mayewski, S. Kipfstuhl, C. Buizert, S. Canessa, R. Dadic, H. A. Kjær, A. Kurbatov, D. Zhang, E. D. Waddington, G. Baccolo, T. Beers, H. J. Brightley, L. Carter, D. Clemens-Sewall, V. G. Ciobanu, B. Delmonte, L. Eling, A. Ellis, S. Ganesh, N. R. Golledge, S. Haines, M. Handley, R. L. Hawley, C. M. Hogan, K. M. Johnson, E. Korotkikh, D. P. Lowry, D. Mandeno, R. M. McKay, J. A. Menking, T. R. Naish, C. Noerling, A. Ollive, A. Orsi, B. C. Proemse, A. R. Pyne, R. L. Pyne, J. Renwick, R. P. Scherer, S. Semper, M. Simonsen, S. B. Sneed, E. J. Steig, A. Tuohy, A. U. Venugopal, F. Valero-Delgado, J. Venkatesh, F. Wang, S. Wang, D. A. Winski, V. H. L. Winton, A. Whiteford, C. Xiao, J. Yang, and X. Zhang. The Ross Sea Dipole – temperature, snow accumulation and sea ice variability in the Ross Sea region, Antarctica, over the past 2700 years. *Climate of the Past*, 14(2):193–214, Feb. 2018. ISSN 1814-9332. https://doi.org/10.5194/cp-14-193-2018. URL https://cp.copernicus.org/articles/14/193/2018/.

T. Blunier. Renland Ice Cap Project (ReCAP) total air content data, Eastern Greenland, 2015, 2024. URL https://arcticdata.io/catalog/view/doi:10.18739/A2ZK55P0N. Medium: text/xml Type: dataset.

https://doi.org/10.5194/egusphere-2026-953
Preprint. Discussion started: 26 March 2026

M. Bock, J. Schmitt, J. Beck, B. Seth, J. Chappellaz, and H. Fischer. Glacial/interglacial wetland, biomass burning, and geologic methane emissions constrained by dual stable isotopic CH_4 ice core records. *Proceedings of the National Academy of Sciences*, 114(29), July 2017. ISSN 0027-8424, 1091-6490. https://doi.org/10.1073/pnas.1613883114. URL https://pnas.org/doi/full/10.1073/pnas.1613883114.

M. Bouchet, A. Landais, A. Grisart, F. Parrenin, F. Prié, R. Jacob, E. Fourré, E. Capron, D. Raynaud, V. Y. Lipenkov, M.-F. Loutre, T. Extier, A. Svensson, E. Legrain, P. Martinerie, M. Leuenberger, W. Jiang, F. Ritterbusch, Z.-T. Lu, and G.-M. Yang. The AICC2023 chronological framework and associated timescale for the EPICA Dome C ice core. preprint, Ice Dynamics/Ice Cores/Milankovitch, May 2023. URL https://egusphere.copernicus.org/preprints/2023/egusphere-2023-1081/.

D. H. Bromwich, J. P. Nicolas, K. M. Hines, J. E. Kay, E. L. Key, M. A. Lazzara, D. Lubin, G. M. McFarquhar, I. V. Gorodetskaya, D. P. Grosvenor, T. Lachlan-Cope, and N. P. M. van Lipzig. Tropospheric clouds in Antarctica. *Reviews of Geophysics*, 50(1):2011RG000363, Mar. 2012. ISSN 8755-1209, 1944-9208. https://doi.org/10.1029/2011RG000363. URL https://agupubs.onlinelibrary.wiley.com/doi/10.1029/2011RG000363.

C. Buizert and J. P. Severinghaus. Dispersion in deep polar firn driven by synoptic-scale surface pressure variability. *The Cryosphere*, 10(5): 2099–2111, Sept. 2016. ISSN 1994-0424. https://doi.org/10.5194/tc-10-2099-2016. URL https://tc.copernicus.org/articles/10/2099/2016/.

C. Buizert, K. M. Cuffey, J. P. Severinghaus, D. Baggenstos, T. J. Fudge, E. J. Steig, B. R. Markle, M. Winstrup, R. H. Rhodes, E. J. Brook, T. A. Sowers, G. D. Clow, H. Cheng, R. L. Edwards, M. Sigl, J. R. McConnell, and K. C. Taylor. The WAIS Divide deep ice core WD2014 chronology – Part 1: Methane synchronization (68–31 ka BP) and the gas age–ice age difference. *Climate of the Past*, 11(2):153–173, Feb. 2015. ISSN 1814-9332. https://doi.org/10.5194/cp-11-153-2015. URL https://cp.copernicus.org/articles/11/153/2015/.

C. Buizert, T. J. Fudge, W. H. G. Roberts, E. J. Steig, S. Sherriff-Tadano, C. Ritz, E. Lefebvre, J. Edwards, K. Kawamura, I. Oyabu, H. Motoyama, E. C. Kahle, T. R. Jones, A. Abe-Ouchi, T. Obase, C. Martin, H. Corr, J. P. Severinghaus, R. Beaudette, J. A. Epifanio, E. J. Brook, K. Martin, J. Chappellaz, S. Aoki, T. Nakazawa, T. A. Sowers, R. B. Alley, J. Ahn, M. Sigl, M. Severi, N. W. Dunbar, A. Svensson, J. M. Fegyveresi, C. He, Z. Liu, J. Zhu, B. L. Otto-Bliesner, V. Y. Lipenkov, M. Kageyama, and J. Schwander. Antarctic surface temperature and elevation during the Last Glacial Maximum. *Science*, 372(6546):1097–1101, June 2021. ISSN 0036-8075, 1095-9203. https://doi.org/10.1126/science.abd2897. URL https://www.science.org/doi/10.1126/science.abd2897.

Z. R. Courville, M. R. Albert, M. A. Fahnestock, L. M. Cathles, and C. A. Shuman. Impacts of an accumulation hiatus on the physical properties of firn at a low-accumulation polar site. *Journal of Geophysical Research: Earth Surface*, 112(F2):2005JF000429, June 2007. ISSN 0148-0227. https://doi.org/10.1029/2005JF000429. URL https://agupubs.onlinelibrary.wiley.com/doi/10.1029/2005JF000429.

K. M. Cuffey. Temperature Reconstruction at the West Antarctic Ice Sheet Divide, 2017. URL http://www.usap-dc.org/view/dataset/600377. Type: dataset.

K. M. Cuffey and W. S. B. Paterson. *The physics of glaciers*. Elsevier, San Diego, fourth edition edition, 2010. ISBN 978-0-12-369461-4 978-0-08-091912-6.

M. Delmotte, D. Raynaud, V. Morgan, and J. Jouzel. Climatic and glaciological information inferred from air-content measurements of a Law Dome (East Antarctica) ice core. *Journal of Glaciology*, 45(150):255–263, 1999. ISSN 0022-1430, 1727-5652. https://doi.org/10.3189/002214399793377031. URL https://www.cambridge.org/core/product/identifier/S0022143000001751/type/journal_article.

J. S. Edwards and J. A. Epifanio. Total air content in ice cores. In *Encyclopedia of Quaternary Science*, pages 176–182. Elsevier, 2025. ISBN 978-0-443-29997-1. https://doi.org/10.1016/B978-0-323-99931-1.00270-1. URL https://linkinghub.elsevier.com/retrieve/pii/B9780323999311002701.

https://doi.org/10.5194/egusphere-2026-953
Preprint. Discussion started: 26 March 2026

O. Eicher, M. Baumgartner, A. Schilt, J. Schmitt, J. Schwander, T. F. Stocker, and H. Fischer. Climatic and insolation control on the high-resolution total air content in the NGRIP ice core. *Climate of the Past*, 12(10):1979–1993, Oct. 2016. ISSN 1814-9332. https://doi.org/10.5194/cp-12-1979-2016. URL https://cp.copernicus.org/articles/12/1979/2016/.

J. A. Epifanio, E. J. Brook, C. Buizert, J. S. Edwards, T. A. Sowers, E. C. Kahle, J. P. Severinghaus, E. J. Steig, D. A. Winski, E. C. Osterberg, T. J. Fudge, M. Aydin, E. Hood, M. Kalk, K. J. Kreutz, D. G. Ferris, and J. A. Kennedy. The SP19 chronology for the South Pole Ice Core – Part 2: gas chronology, Δage, and smoothing of atmospheric records. *Climate of the Past*, 16(6):2431–2444, Dec. 2020. ISSN 1814-9332. https://doi.org/10.5194/cp-16-2431-2020. URL https://cp.copernicus.org/articles/16/2431/2020/.

J. A. Epifanio, E. J. Brook, C. Buizert, E. C. Pettit, J. S. Edwards, J. M. Fegyveresi, T. A. Sowers, J. P. Severinghaus, and E. C. Kahle. Millennial and orbital-scale variability in a 54,000-year record of total air content from the South Pole ice core, May 2023. URL https://egusphere.copernicus.org/preprints/2023/egusphere-2023-578/.

J. M. Fegyveresi. *Physical properties of the West Antarctic Ice Sheet (WAIS) Divide deep core: Development, evolution, and interpretation*. PhD thesis, The Pennsylvania State University, University Park, PA, 2015. UMI: 37155012015.

M. *Fisher, T. *Stafford, T. Moon, and A. Thurber. QGreenland, Sept. 2023. URL https://zenodo.org/record/8326507.

J. Freitag, F. Wilhelms, and S. Kipfstuhl. Microstructure-dependent densification of polar firn derived from X-ray microtomography. *Journal of Glaciology*, 50(169):243–250, 2004. ISSN 0022-1430, 1727-5652. https://doi.org/10.3189/172756504781830123. URL https://www.cambridge.org/core/product/identifier/S0022143000214317/type/journal_article.

T. J. Fudge, B. R. Markle, K. M. Cuffey, C. Buizert, K. C. Taylor, E. J. Steig, E. D. Waddington, H. Conway, and M. Koutnik. Variable relationship between accumulation and temperature in West Antarctica for the past 31,000 years. *Geophysical Research Letters*, 43(8):3795–3803, Apr. 2016. ISSN 0094-8276, 1944-8007. https://doi.org/10.1002/2016GL068356. URL https://agupubs.onlinelibrary.wiley.com/doi/10.1002/2016GL068356.

E. Gautier, J. Savarino, J. Erbland, A. Lanciki, and P. Possenti. Variability of sulfate signal in ice core records based on five replicate cores. *Climate of the Past*, 12(1):103–113, Jan. 2016. ISSN 1814-9332. https://doi.org/10.5194/cp-12-103-2016. URL https://cp.copernicus.org/articles/12/103/2016/.

C. Goujon, J. Barnola, and C. Ritz. Modeling the densification of polar firn including heat diffusion: Application to close-off characteristics and gas isotopic fractionation for Antarctica and Greenland sites. *Journal of Geophysical Research: Atmospheres*, 108(D24):2002JD003319, Dec. 2003. ISSN 0148-0227. https://doi.org/10.1029/2002JD003319. URL https://agupubs.onlinelibrary.wiley.com/doi/10.1029/2002JD003319.

A. J. Gow. On the Rates of Growth of Grains and Crystals in South Polar Firn. *Journal of Glaciology*, 8(53):241–252, 1969. ISSN 0022-1430, 1727-5652. https://doi.org/10.3189/S0022143000031233. URL https://www.cambridge.org/core/product/identifier/S0022143000031233/type/journal_article.

S. A. Gregory, M. R. Albert, and I. Baker. Impact of physical properties and accumulation rate on pore close-off in layered firn. *The Cryosphere*, 8(1):91–105, Jan. 2014. ISSN 1994-0424. https://doi.org/10.5194/tc-8-91-2014. URL https://tc.copernicus.org/articles/8/91/2014/.

C. U. Hammer and D. Dahl-Jensen. GRIP Accumulation Rates, 1999. URL https://doi.org/10.1594/PANGAEA.55084. Type: dataset.

R. Harris Stuart. *Evolution of snow and air below the surface of the East Antarctic ice sheet*. PhD thesis, Université Paris Saclay, May 2024. URL https://theses.hal.science/tel-04996074/.

R. Harris Stuart, A. Landais, L. Arnaud, C. Buizert, E. Capron, M. Dumont, Q. Libois, R. Mulvaney, A. Orsi, G. Picard, F. Prié, J. Severinghaus, B. Stenni, and P. Martinerie. On the relationship between δ O_2 N_2 variability and ice sheet surface conditions

https://doi.org/10.5194/egusphere-2026-953
Preprint. Discussion started: 26 March 2026

in Antarctica. *The Cryosphere*, 18(8):3741–3763, Aug. 2024. ISSN 1994-0424. https://doi.org/10.5194/tc-18-3741-2024. URL https://tc.copernicus.org/articles/18/3741/2024/.

M. Hörhold, T. Laepple, J. Freitag, M. Bigler, H. Fischer, and S. Kipfstuhl. On the impact of impurities on the densification of polar firn. *Earth and Planetary Science Letters*, 325-326:93–99, Apr. 2012. ISSN 0012821X. https://doi.org/10.1016/j.epsl.2011.12.022. URL https://linkinghub.elsevier.com/retrieve/pii/S0012821X11007424.

M. W. Hörhold, S. Kipfstuhl, F. Wilhelms, J. Freitag, and A. Frenzel. The densification of layered polar firn: DENSITY VARIABILITY. *Journal of Geophysical Research: Earth Surface*, 116(F1):n/a–n/a, Mar. 2011. ISSN 01480227. https://doi.org/10.1029/2009JF001630. URL http://doi.wiley.com/10.1029/2009JF001630.

S. J. Johnsen. GRIP Temperature Profile, 2003. URL https://doi.org/10.1594/PANGAEA.89007. Type: dataset.

J. Jouzel, V. Masson-Delmotte, O. Cattani, G. Dreyfus, S. Falourd, G. Hoffmann, B. Minster, J. Nouet, J. M. Barnola, J. Chappellaz, H. Fischer, J. C. Gallet, S. Johnsen, M. Leuenberger, L. Loulergue, D. Luethi, H. Oerter, F. Parrenin, G. Raisbeck, D. Raynaud, A. Schilt, J. Schwander, E. Selmo, R. Souchez, R. Spahni, B. Stauffer, J. P. Steffensen, B. Stenni, T. F. Stocker, J. L. Tison, M. Werner, and E. W. Wolff. Orbital and Millennial Antarctic Climate Variability over the Past 800,000 Years. *Science*, 317(5839):793–796, Aug. 2007. ISSN 0036-8075, 1095-9203. https://doi.org/10.1126/science.1141038. URL https://www.science.org/doi/10.1126/science.1141038.

E. C. Kahle, E. J. Steig, T. R. Jones, T. J. Fudge, M. R. Koutnik, V. A. Morris, B. H. Vaughn, A. J. Schauer, C. M. Stevens, H. Conway, E. D. Waddington, C. Buizert, J. Epifanio, and J. W. C. White. Reconstruction of Temperature, Accumulation Rate, and Layer Thinning From an Ice Core at South Pole, Using a Statistical Inverse Method. *Journal of Geophysical Research: Atmospheres*, 126(13):e2020JD033300, July 2021. ISSN 2169-897X, 2169-8996. https://doi.org/10.1029/2020JD033300. URL https://agupubs.onlinelibrary.wiley.com/doi/10.1029/2020JD033300.

K. Kawamura, F. Parrenin, L. Lisiecki, R. Uemura, F. Vimeux, J. P. Severinghaus, M. A. Hutterli, T. Nakazawa, S. Aoki, J. Jouzel, M. E. Raymo, K. Matsumoto, H. Nakata, H. Motoyama, S. Fujita, K. Goto-Azuma, Y. Fujii, and O. Watanabe. Northern Hemisphere forcing of climatic cycles in Antarctica over the past 360,000 years. *Nature*, 448(7156):912–916, Aug. 2007. ISSN 0028-0836, 1476-4687. https://doi.org/10.1038/nature06015. URL https://www.nature.com/articles/nature06015.

V. A. Khomyakova, N. A. Tebenkova, V. Y. Lipenkov, and D. Raynaud. Consistency of the Orbital Chronologies Derived for Vostok and EPICA DC Ice Cores Based on the Dependence of Ice Air Content on Local Insolation. *Izvestiya, Atmospheric and Oceanic Physics*, 61 (S2):S135–S144, Dec. 2025. ISSN 0001-4338, 1555-628X. https://doi.org/10.1134/S0001433825701270. URL https://link.springer.com/10.1134/S0001433825701270.

P. Kindler, M. Guillevic, M. Baumgartner, J. Schwander, A. Landais, and M. Leuenberger. Temperature reconstruction from 10 to 120 kyr b2k from the NGRIP ice core. *Climate of the Past*, 10(2):887–902, Apr. 2014. ISSN 1814-9332. https://doi.org/10.5194/cp-10-887-2014. URL https://cp.copernicus.org/articles/10/887/2014/.

J. E. Lee, E. J. Brook, N. A. N. Bertler, C. Buizert, T. Baisden, T. Blunier, V. G. Ciobanu, H. Conway, D. Dahl-Jensen, T. J. Fudge, R. Hindmarsh, E. D. Keller, F. Parrenin, J. P. Severinghaus, P. Vallelonga, E. D. Waddington, and M. Winstrup. An 83 000-year-old ice core from Roosevelt Island, Ross Sea, Antarctica. *Climate of the Past*, 16(5):1691–1713, Sept. 2020. ISSN 1814-9332. https://doi.org/10.5194/cp-16-1691-2020. URL https://cp.copernicus.org/articles/16/1691/2020/.

V. Lipenkov, F. Candaudap, J. Ravoire, E. Dulac, and D. Raynaud. A new device for the measurement of air content in polar ice. *Journal of Glaciology*, 41(138):423–429, 1995. ISSN 0022-1430, 1727-5652. https://doi.org/10.3189/S0022143000016294. URL https://www.cambridge.org/core/product/identifier/S0022143000016294/type/journal_article.

https://doi.org/10.5194/egusphere-2026-953
Preprint. Discussion started: 26 March 2026

V. Lipenkov, D. Raynaud, M. Loutre, and P. Duval. On the potential of coupling air content and O2/N2 from trapped air for establishing an ice core chronology tuned on local insolation. *Quaternary Science Reviews*, 30(23-24):3280–3289, Nov. 2011. ISSN 02773791. https://doi.org/10.1016/j.quascirev.2011.07.013. URL https://linkinghub.elsevier.com/retrieve/pii/S0277379111002174.

L. Loulergue, A. Schilt, R. Spahni, V. Masson-Delmotte, T. Blunier, B. Lemieux, J.-M. Barnola, D. Raynaud, T. F. Stocker, and J. Chappellaz. Orbital and millennial-scale features of atmospheric CH4 over the past 800,000 years. *Nature*, 453(7193):383–386, May 2008. ISSN 0028-0836, 1476-4687. https://doi.org/10.1038/nature06950. URL https://www.nature.com/articles/nature06950.

G. J. Marshall, D. W. J. Thompson, and M. R. van den Broeke. The Signature of Southern Hemisphere Atmospheric Circulation Patterns in Antarctic Precipitation. *Geophysical Research Letters*, 44(22), Nov. 2017. ISSN 0094-8276, 1944-8007. https://doi.org/10.1002/2017GL075998. URL https://agupubs.onlinelibrary.wiley.com/doi/10.1002/2017GL075998.

P. Martinerie, D. Raynaud, D. Mazaudier, A. J. Gow, G. Holdsworth, V. Y. Lipenkov, and N. W. Young. The Relationship Between Total Gas Content of Polar Ice, Atmospheric Pressure and Surface Elevation (Abstract). *Annals of Glaciology*, 11:203–203, 1988. ISSN 0260-3055, 1727-5644. https://doi.org/10.3189/S0260305500006613. URL https://www.cambridge.org/core/product/identifier/S0260305500006613/type/journal_article.

P. Martinerie, V. Lipenkov, and D. Raynaud. Correction Of Air-content Measurements In Polar Ice For The Effect Of Cut Bubbles At The Surface Of The Sample. *Journal of Glaciology*, 36(124):299–303, 1990. ISSN 0022-1430, 1727-5652. https://doi.org/10.3189/002214390793701282. URL https://www.cambridge.org/core/product/identifier/S0022143000004329/type/journal_article.

P. Martinerie, D. Raynaud, D. M. Etheridge, J.-M. Barnola, and D. Mazaudier. Physical and climatic parameters which influence the air content in polar ice. *Earth and Planetary Science Letters*, 112(1-4):1–13, Aug. 1992. ISSN 0012821X. https://doi.org/10.1016/0012-821X(92)90002-D. URL https://linkinghub.elsevier.com/retrieve/pii/0012821X9290002D.

P. Martinerie, V. Y. Lipenkov, D. Raynaud, J. Chappellaz, N. I. Barkov, and C. Lorius. Air content paleo record in the Vostok ice core (Antarctica): A mixed record of climatic and glaciological parameters. *Journal of Geophysical Research*, 99(D5):10565, 1994. ISSN 0148-0227. https://doi.org/10.1029/93JD03223. URL http://doi.wiley.com/10.1029/93JD03223.

K. Matsuoka, A. Skoglund, G. Roth, J. de Pomereu, H. Griffiths, R. Headland, B. Herried, K. Katsumata, A. Le Brocq, K. Licht, F. Morgan, P. D. Neff, C. Ritz, M. Scheinert, T. Tamura, A. Van de Putte, M. van den Broeke, A. von Deschwanden, C. Deschamps-Berger, B. Van Liefferinge, S. Tronstad, and Y. Melvær. Quantarctica, an integrated mapping environment for Antarctica, the Southern Ocean, and sub-Antarctic islands. *Environmental Modelling & Software*, 140:105015, June 2021. ISSN 13648152. https://doi.org/10.1016/j.envsoft.2021.105015. URL https://linkinghub.elsevier.com/retrieve/pii/S136481522100058X.

J. A. Mischler, T. A. Sowers, R. B. Alley, M. Battle, J. R. McConnell, L. Mitchell, T. Popp, E. Sofen, and M. K. Spencer. Carbon and hydrogen isotopic composition of methane over the last 1000 years. *Global Biogeochemical Cycles*, 23(4):2009GB003460, Dec. 2009. ISSN 0886-6236, 1944-9224. https://doi.org/10.1029/2009GB003460. URL https://agupubs.onlinelibrary.wiley.com/doi/10.1029/2009GB003460.

L. E. Mitchell, C. Buizert, E. J. Brook, D. J. Breton, J. Fegyveresi, D. Baggenstos, A. Orsi, J. Severinghaus, R. B. Alley, M. Albert, R. H. Rhodes, J. R. McConnell, M. Sigl, O. Maselli, S. Gregory, and J. Ahn. Observing and modeling the influence of layering on bubble trapping in polar firn. *Journal of Geophysical Research: Atmospheres*, 120(6):2558–2574, Mar. 2015. ISSN 2169-897X, 2169-8996. https://doi.org/10.1002/2014JD022766. URL https://agupubs.onlinelibrary.wiley.com/doi/10.1002/2014JD022766.

T. Moon, M. Fisher, T. Stafford, and L. Harden. QGreenland, Sept. 2023. URL https://zenodo.org/doi/10.5281/zenodo.12823307. Version Number: 3.0.0 Type: dataset.

https://doi.org/10.5194/egusphere-2026-953
Preprint. Discussion started: 26 March 2026

R. Mulvaney, J. Rix, S. Polfrey, M. Grieman, C. Martìn, C. Nehrbass-Ahles, I. Rowell, R. Tuckwell, and E. Wolff. Ice drilling on Skytrain Ice Rise and Sherman Island, Antarctica. *Annals of Glaciology*, 62(85-86):311–323, Sept. 2021. ISSN 0260-3055, 1727-5644. https://doi.org/10.1017/aog.2021.7. URL https://www.cambridge.org/core/product/identifier/S0260305521000070/type/journal_article.

NEEM community members. Eemian interglacial reconstructed from a Greenland folded ice core. *Nature*, 493(7433):489–494, Jan. 2013. ISSN 0028-0836, 1476-4687. https://doi.org/10.1038/nature11789. URL https://www.nature.com/articles/nature11789.

L. Nicola, D. Notz, and R. Winkelmann. Revisiting temperature sensitivity: how does Antarctic precipitation change with temperature? *The Cryosphere*, 17(7):2563–2583, July 2023. ISSN 1994-0424. https://doi.org/10.5194/tc-17-2563-2023. URL https://tc.copernicus.org/articles/17/2563/2023/.

I. Oyabu, K. Kawamura, K. Kitamura, R. Dallmayr, A. Kitamura, C. Sawada, J. P. Severinghaus, R. Beaudette, A. Orsi, S. Sugawara, S. Ishidoya, D. Dahl-Jensen, K. Goto-Azuma, S. Aoki, and T. Nakazawa. New technique for high-precision, simultaneous measurements of CH_4 , N_2 O and CO_2 concentrations; isotopic and elemental ratios of N_2 , O_2 and Ar; and total air content in ice cores by wet extraction. *Atmospheric Measurement Techniques*, 13(12):6703–6731, Dec. 2020. ISSN 1867-8548. https://doi.org/10.5194/amt-13-6703-2020. URL https://amt.copernicus.org/articles/13/6703/2020/.

I. Oyabu, K. Kawamura, C. Buizert, F. Parrenin, A. Orsi, K. Kitamura, S. Aoki, and T. Nakazawa. The Dome Fuji ice core DF2021 chronology (0–207 kyr BP). *Quaternary Science Reviews*, 294:107754, Oct. 2022. ISSN 02773791. https://doi.org/10.1016/j.quascirev.2022.107754. URL https://linkinghub.elsevier.com/retrieve/pii/S0277379122003857.

F. Parrenin, G. Dreyfus, G. Durand, S. Fujita, O. Gagliardini, F. Gillet, J. Jouzel, K. Kawamura, N. Lhomme, V. Masson-Delmotte, C. Ritz, J. Schwander, H. Shoji, R. Uemura, O. Watanabe, and N. Yoshida. 1-D-ice flow modelling at EPICA Dome C and Dome Fuji, East Antarctica. *Climate of the Past*, 3(2):243–259, June 2007. ISSN 1814-9332. https://doi.org/10.5194/cp-3-243-2007. URL https://cp.copernicus.org/articles/3/243/2007/.

Past Interglacials Working Group of PAGES. Interglacials of the last 800,000 years. *Reviews of Geophysics*, 54(1):162–219, Mar. 2016. ISSN 8755-1209, 1944-9208. https://doi.org/10.1002/2015RG000482. URL https://agupubs.onlinelibrary.wiley.com/doi/10.1002/2015RG000482.

J. R. Petit, J. Jouzel, D. Raynaud, N. I. Barkov, G. Delaygue, M. Delmotte, V. M. Kotlyakov, M. Legrand, V. Y. Lipenkov, C. Lorius, and E. Saltzman. Climate and atmospheric history of the past 420,000 years from the Vostok ice core, Antarctica. 399, 1999.

S. O. Rasmussen, A. M. Svensson, and B. M. Vinther. Greenland Ice-Core Chronology 2005 (GICC05) annual layer depths for various Greenland ice cores, 2022. URL https://doi.org/10.1594/PANGAEA.943195. Type: dataset bundled publication.

M. E. Raymo and K. H. Nisancioglu. The 41 kyr world: Milankovitch's other unsolved mystery. *Paleoceanography*, 18(1):2002PA000791, Mar. 2003. ISSN 0883-8305, 1944-9186. https://doi.org/10.1029/2002PA000791. URL https://agupubs.onlinelibrary.wiley.com/doi/10.1029/2002PA000791.

D. Raynaud and B. Lebel. Total gas content and surface elevation of polar ice sheets. *Nature*, 281(5729):289–291, Sept. 1979. ISSN 0028-0836, 1476-4687. https://doi.org/10.1038/281289a0. URL https://www.nature.com/articles/281289a0.

D. Raynaud and C. Lorius. Climatic Implications of Total Gas Content in Ice at Camp Century. *Nature*, 243(5405):283–284, June 1973. ISSN 0028-0836, 1476-4687. https://doi.org/10.1038/243283a0. URL https://www.nature.com/articles/243283a0.

D. Raynaud, R. Delmas, J. Ascencio, and M. Legrand. Gas Extraction From Polar Ice Cores: A Critical Issue For Studying The Evolution of Atmospheric CO_2 and Ice-Sheet Surface Elevation. *Annals of Glaciology*, 3:265–268, 1982. ISSN 0260-3055, 1727-5644. https://doi.org/10.3189/S0260305500002895. URL https://www.cambridge.org/core/product/identifier/S0260305500002895/type/journal_article.

https://doi.org/10.5194/egusphere-2026-953
Preprint. Discussion started: 26 March 2026

D. Raynaud, J. Chappellaz, C. Ritz, and P. Martinerie. Air content along the Greenland Ice Core Project core: A record of surface climatic parameters and elevation in central Greenland. *Journal of Geophysical Research: Oceans*, 102(C12):26607–26613, Nov. 1997. ISSN 0148-0227. https://doi.org/10.1029/97JC01908. URL https://agupubs.onlinelibrary.wiley.com/doi/10.1029/97JC01908.

D. Raynaud, V. Lipenkov, B. Lemieux-Dudon, P. Duval, M.-F. Loutre, and N. Lhomme. The local insolation signature of air content in Antarctic ice. A new step toward an absolute dating of ice records. *Earth and Planetary Science Letters*, 261(3-4):337–349, Sept. 2007. ISSN 0012821X. https://doi.org/10.1016/j.epsl.2007.06.025. URL https://linkinghub.elsevier.com/retrieve/pii/S0012821X0700413X.

D. Raynaud, Q. Yin, E. Capron, Z. Wu, F. Parrenin, A. Berger, and V. Lipenkov. Local summer temperature changes over the past 440 ka revealed by the total air content in the Antarctic EPICA Dome C ice core. *Climate of the Past*, 20(6):1269–1282, June 2024. ISSN 1814-9332. https://doi.org/10.5194/cp-20-1269-2024. URL https://cp.copernicus.org/articles/20/1269/2024/.

C. F. Schaller, J. Freitag, and O. Eisen. Critical porosity of gas enclosure in polar firn independent of climate. *Climate of the Past*, 13 (11):1685–1693, Nov. 2017. ISSN 1814-9332. https://doi.org/10.5194/cp-13-1685-2017. URL https://cp.copernicus.org/articles/13/1685/2017/.

J. Schmitt, R. Schneider, and H. Fischer. A sublimation technique for high-precision measurements of δ^{13} CO_2 and mixing ratios of CO_2 and N_2 O from air trapped in ice cores. *Atmospheric Measurement Techniques*, 4(7):1445–1461, July 2011. ISSN 1867-8548. https://doi.org/10.5194/amt-4-1445-2011. URL https://amt.copernicus.org/articles/4/1445/2011/.

J. Schmitt, B. Seth, M. Bock, and H. Fischer. Online technique for isotope and mixing ratios of CH_4 , N_2 O, Xe and mixing ratios of organic trace gases on a single ice core sample. *Atmospheric Measurement Techniques*, 7(8):2645–2665, Aug. 2014. ISSN 1867-8548. https://doi.org/10.5194/amt-7-2645-2014. URL https://amt.copernicus.org/articles/7/2645/2014/.

J. Schwander and B. Stauffer. Age difference between polar ice and the air trapped in its bubbles. *Nature*, 311(5981):45–47, Sept. 1984. ISSN 0028-0836, 1476-4687. https://doi.org/10.1038/311045a0. URL https://www.nature.com/articles/311045a0.

J. P. Severinghaus, A. Grachev, and M. Battle. Thermal fractionation of air in polar firn by seasonal temperature gradients. *Geochemistry, Geophysics, Geosystems*, 2(7):2000GC000146, July 2001. ISSN 1525-2027, 1525-2027. https://doi.org/10.1029/2000GC000146. URL https://agupubs.onlinelibrary.wiley.com/doi/10.1029/2000GC000146.

A. Skakun and V. Y. Lipenkov. Assessing the uncertainties of an ice core time scale based on orbital tuning of air content records: a case study of the Dome Fuji (Antarctica) ice core. (in russian). *Arctic and Antarctic Research*, pages 14–29, 2016. ISSN 2618-6713.

T. Sowers, M. Bender, D. Raynaud, and Y. S. Korotkevich. δ^{15} N of N_2 in air trapped in polar ice: A tracer of gas transport in the firn and a possible constraint on ice age-gas age differences. *Journal of Geophysical Research: Atmospheres*, 97(D14):15683–15697, Oct. 1992. ISSN 0148-0227. https://doi.org/10.1029/92JD01297. URL https://agupubs.onlinelibrary.wiley.com/doi/10.1029/92JD01297.

B. Stauffer, J. Schwander, and H. Oeschger. Enclosure of Air During Metamorphosis of Dry Firn to Ice. *Annals of Glaciology*, 6:108–112, 1985. ISSN 0260-3055, 1727-5644. https://doi.org/10.3189/1985AoG6-1-108-112. URL https://www.cambridge.org/core/product/identifier/S0260305500010119/type/journal_article.

B. Stenni, M. Proposito, R. Gragnani, O. Flora, J. Jouzel, S. Falourd, and M. Frezzotti. Eight centuries of volcanic signal and climate change at Talos Dome (East Antarctica). *Journal of Geophysical Research: Atmospheres*, 107(D9), May 2002. ISSN 0148-0227. https://doi.org/10.1029/2000JD000317. URL https://agupubs.onlinelibrary.wiley.com/doi/10.1029/2000JD000317.

B. Stenni, V. Masson-Delmotte, E. Selmo, H. Oerter, H. Meyer, R. Röthlisberger, J. Jouzel, O. Cattani, S. Falourd, H. Fischer, G. Hoffmann, P. Iacumin, S. Johnsen, B. Minster, and R. Udisti. The deuterium excess records of EPICA Dome C and Dronning Maud Land ice cores (East Antarctica). *Quaternary Science Reviews*, 29(1-2):146–159, Jan. 2010. ISSN 02773791. https://doi.org/10.1016/j.quascirev.2009.10.009. URL https://linkinghub.elsevier.com/retrieve/pii/S0277379109003540.

https://doi.org/10.5194/egusphere-2026-953
Preprint. Discussion started: 26 March 2026

B. Stenni, C. Scarchilli, V. Masson-Delmotte, E. Schlosser, V. Ciardini, G. Dreossi, P. Grigioni, M. Bonazza, A. Cagnati, D. Karlicek, C. Risi, R. Udisti, and M. Valt. Three-year monitoring of stable isotopes of precipitation at ConcordiaStation, East Antarctica. *The Cryosphere*, 10(5):2415–2428, Oct. 2016. ISSN 1994-0424. https://doi.org/10.5194/tc-10-2415-2016. URL https://tc.copernicus.org/articles/10/2415/2016/.

R. Uemura, H. Motoyama, V. Masson-Delmotte, J. Jouzel, K. Kawamura, K. Goto-Azuma, S. Fujita, T. Kuramoto, M. Hirabayashi, T. Miyake, H. Ohno, K. Fujita, A. Abe-Ouchi, Y. Iizuka, S. Horikawa, M. Igarashi, K. Suzuki, T. Suzuki, and Y. Fujii. Asynchrony between Antarctic temperature and CO2 associated with obliquity over the past 720,000 years. *Nature Communications*, 9(1):961, Mar. 2018. ISSN 2041-1723. https://doi.org/10.1038/s41467-018-03328-3. URL https://www.nature.com/articles/s41467-018-03328-3.

B. M. Vinther, H. B. Clausen, S. J. Johnsen, S. O. Rasmussen, K. K. Andersen, S. L. Buchardt, D. Dahl-Jensen, I. K. Seierstad, M. Siggaard-Andersen, J. P. Steffensen, A. Svensson, J. Olsen, and J. Heinemeier. A synchronized dating of three Greenland ice cores throughout the Holocene. *Journal of Geophysical Research: Atmospheres*, 111(D13):2005JD006921, July 2006. ISSN 0148-0227. https://doi.org/10.1029/2005JD006921. URL https://agupubs.onlinelibrary.wiley.com/doi/10.1029/2005JD006921.

S. Vudayagiri, B. Vinther, J. Freitag, P. L. Langen, and T. Blunier. Total air content measurements from the RECAP ice core. *Climate of the Past*, 21(2):517–528, Feb. 2025. ISSN 1814-9332. https://doi.org/10.5194/cp-21-517-2025. URL https://cp.copernicus.org/articles/21/517/2025/.

WAIS Divide Project Members. Onset of deglacial warming in West Antarctica driven by local orbital forcing. *Nature*, 500(7463):440–444, Aug. 2013. ISSN 0028-0836, 1476-4687. https://doi.org/10.1038/nature12376. URL https://www.nature.com/articles/nature12376.

Y. Wang, X. Zhang, W. Ning, M. A. Lazzara, M. Ding, C. H. Reijmer, P. C. J. P. Smeets, P. Grigioni, P. Heil, E. R. Thomas, D. Mikolajczyk, L. J. Welhouse, L. M. Keller, Z. Zhai, Y. Sun, and S. Hou. The AntAWS dataset: a compilation of Antarctic automatic weather station observations. *Earth System Science Data*, 15(1):411–429, Jan. 2023. ISSN 1866-3516. https://doi.org/10.5194/essd-15-411-2023. URL https://essd.copernicus.org/articles/15/411/2023/.

O. Watanabe, K. Kamiyama, H. Motoyama, Y. Fujii, H. Shoji, and K. Satow. The paleoclimate record in the ice core at Dome Fuji station, East Antarctica. *Annals of Glaciology*, 29:176–178, 1999. ISSN 0260-3055, 1727-5644. https://doi.org/10.3189/172756499781821553. URL https://www.cambridge.org/core/product/identifier/S0260305500267608/type/journal_article.

J. D. Wille, V. Favier, I. V. Gorodetskaya, C. Agosta, C. Kittel, J. C. Beeman, N. C. Jourdain, J. T. M. Lenaerts, and F. Codron. Antarctic Atmospheric River Climatology and Precipitation Impacts. *Journal of Geophysical Research: Atmospheres*, 126(8):e2020JD033788, Apr. 2021. ISSN 2169-897X, 2169-8996. https://doi.org/10.1029/2020JD033788. URL https://agupubs.onlinelibrary.wiley.com/doi/10.1029/2020JD033788.

D. A. Winski, T. J. Fudge, D. G. Ferris, E. C. Osterberg, J. M. Fegyveresi, J. Cole-Dai, Z. Thundercloud, T. S. Cox, K. J. Kreutz, N. Ortman, C. Buizert, J. Epifanio, E. J. Brook, R. Beaudette, J. Severinghaus, T. Sowers, E. J. Steig, E. C. Kahle, T. R. Jones, V. Morris, M. Aydin, M. R. Nicewonger, K. A. Casey, R. B. Alley, E. D. Waddington, N. A. Iverson, N. W. Dunbar, R. C. Bay, J. M. Souney, M. Sigl, and J. R. McConnell. The SP19 chronology for the South Pole Ice Core – Part 1: volcanic matching and annual layer counting. *Climate of the Past*, 15(5):1793–1808, Oct. 2019. ISSN 1814-9332. https://doi.org/10.5194/cp-15-1793-2019. URL https://cp.copernicus.org/articles/15/1793/2019/.

M. Winstrup, P. Vallelonga, H. A. Kjær, T. J. Fudge, J. E. Lee, M. H. Riis, R. Edwards, N. A. N. Bertler, T. Blunier, E. J. Brook, C. Buizert, G. Ciobanu, H. Conway, D. Dahl-Jensen, A. Ellis, B. D. Emanuelsson, R. C. A. Hindmarsh, E. D. Keller, A. V. Kurbatov, P. A. Mayewski, P. D. Neff, R. L. Pyne, M. F. Simonsen, A. Svensson, A. Tuohy, E. D. Waddington, and S. Wheatley. A 2700-year annual timescale

https://doi.org/10.5194/egusphere-2026-953
Preprint. Discussion started: 26 March 2026

and accumulation history for an ice core from Roosevelt Island, West Antarctica. *Climate of the Past*, 15(2):751–779, Apr. 2019. ISSN 1814-9332. https://doi.org/10.5194/cp-15-751-2019. URL https://cp.copernicus.org/articles/15/751/2019/.

E. W. Wolff, H. Fischer, F. Fundel, U. Ruth, B. Twarloh, G. C. Littot, R. Mulvaney, R. Röthlisberger, M. de Angelis, C. F. Boutron, M. Hansson, U. Jonsell, M. A. Hutterli, F. Lambert, P. Kaufmann, B. Stauffer, T. F. Stocker, J. P. Steffensen, M. Bigler, M. L. Siggaard-Andersen, R. Udisti, S. Becagli, E. Castellano, M. Severi, D. Wagenbach, C. Barbante, P. Gabrielli, and V. Gaspari. Southern Ocean sea-ice extent, productivity and iron flux over the past eight glacial cycles. *Nature*, 440(7083):491–496, Mar. 2006. ISSN 0028-0836, 1476-4687. https://doi.org/10.1038/nature04614. URL https://www.nature.com/articles/nature04614.

E. W. Wolff, C. Nehrbass-Ahles, A. C. F. King, and T. K. Bauska. Total air content data for the Skytrain Ice Rise ice core, 2024. URL https://doi.pangaea.de/10.1594/PANGAEA.973190. Artwork Size: 2257 data points Medium: text/tab-separated-values Pages: 2257 data points Type: dataset.

Q. Z. Yin, Z. P. Wu, A. Berger, H. Goosse, and D. Hodell. Insolation triggered abrupt weakening of Atlantic circulation at the end of interglacials. *Science*, 373(6558):1035–1040, Aug. 2021. ISSN 0036-8075, 1095-9203. https://doi.org/10.1126/science.abg1737. URL https://www.science.org/doi/10.1126/science.abg1737.

D. York, N. M. Evensen, M. L. Martı´nez, and J. De Basabe Delgado. Unified equations for the slope, intercept, and standard errors of the best straight line. *American Journal of Physics*, 72(3):367–375, Mar. 2004. ISSN 0002-9505, 1943-2909. https://doi.org/10.1119/1.1632486. URL https://pubs.aip.org/ajp/article/72/3/367/1042020/Unified-equations-for-the-slope-intercept-and.